Basin Research

IAS EAGE

Basin Research (2014)1–26, doi: 10.1111/bre.12076

Event sedimentation in low-latitude deep-water carbonate basins, Anegada passage, northeast Caribbean

Jason D. Chaytor and Uri S. ten Brink

U.S. Geological Survey, USGS Woods Hole Coastal and Marine Science Center, Woods Hole, MA, USA

ABSTRACT

The Virgin Islands and Whiting basins in the Northeast Caribbean are deep, structurally controlled depocentres partially bound by shallow-water carbonate platforms. Closed basins such as these are thought to document earthquake and hurricane events through the accumulation of event layers such as debris flow and turbidity current deposits and the internal deformation of deposited material. Event layers in the Virgin Islands and Whiting basins are predominantly thin and discontinuous, containing varying amounts of reef- and slope-derived material. Three turbidites/sandy intervals in the upper 2 m of sediment in the eastern Virgin Islands Basin were deposited between *ca*. 2000 and 13 600 years ago, but do not extend across the basin. In the central and western Virgin Islands Basin, a structureless clay-rich interval is interpreted to be a unifite. Within the Whiting Basin, several discontinuous turbidites and other sand-rich intervals are primarily deposited in base of slope fans. The youngest of these turbidites is *ca*. 2600 years old. Sediment accumulation in these basins is low (<0.1 mm year^{-1}) for basin adjacent to carbonate platform, possibly due to limited sediment input during highstand sea-level conditions, sediment trapping and/or cohesive basin walls. We find no evidence of recent sediment transport (turbidites or debris flows) or sediment deformation that can be attributed to the *ca*. M7.2 1867 Virgin Islands earthquake whose epicentre was located on the north wall of the Virgin Islands Basin or to recent hurricanes that have impacted the region. The lack of significant appreciable pebble or greater size carbonate material in any of the available cores suggests that submarine landslide and basin-wide blocky debris flows have not been a significant mechanism of basin margin modification in the last several thousand years. Thus, basins such as those described here may be poor recorders of past natural hazards, but may provide a long-term record of past oceanographic conditions in ocean passages.

INTRODUCTION

Carbonate reefs and platforms produce substantial quantities of sediment that are often in excess of their accommodation capacity (Handford & Loucks, 1993; Andresen *et al.*, 2003; Jorry *et al.*, 2010). These excess sediments, along with those on the slope below the platforms, are transported into deep-water depositional environments primarily through turbidity currents and slope failures triggered by earthquakes, storms and sediment overloading (see Masson *et al.*, 2006). The depositional history of restricted basins at the base of these slopes may record the long-term earthquake history of a region. Event histories have been successfully established using this technique in lacustrine (e.g. Inouchi *et al.*, 1996; Strasser *et al.*, 2007), fjord (e.g. St-Onge *et al.*, 2004) and marginal sea (e.g. Sar & Ça Atay, 2006) environments.

Correspondence: Jason Chaytor, U.S. Geological Survey, USGS Woods Hole Coastal and Marine Science Center, Woods Hole, MA 02543, USA. E-mail: jchaytor@usgs.gov

Transport of platform and reef sediments occurs via two mechanisms: (1) as line sources, where debris is shed along an extended portion or the entire length of the platform, and/or (2) via point sources, such as openings in platform-edge reefs, leading to slope channel and basin floor fan morphologies similar to that of mature siliciclastic margins (Crevello & Schlager, 1980; Mulder *et al.*, 2012). The addition of these platform and reef sediments to slope-sourced material and the continuous rain of pelagic flux, leads to the development of complex platform–basin transition, slope, and basin facies (see McIlreath & James, 1978), the understanding of which can provide valuable information into both the short and long-term geological development of these regions.

Studies of deep-water basins adjacent to modern carbonate platforms show that they contain a complex pattern of either basin-wide or marginal debris flow and turbidite deposits intercalated with thin, discontinuous sand layers and pelagic muds (e.g. Bornhold & Pilkey, 1971; Seiglie *et al.*, 1976; Ditty *et al.*, 1977; Schlager & Chermak, 1979; Crevello & Schlager, 1980; Droxler & Schlager, 1985; Andresen *et al.*, 2003; Jorry *et al.*, 2008;

Webster *et al.*, 2012). The continuity, thickness, and composition of the sand and pelagic intervals within these basins have been used to determine the source area characteristics, transport-initiating trigger events, and how the basin morphology interacts with individual flows to affect their transport.

Climate processes and tectonic environment have been shown to strongly control the nature of basin floor sediments (Pilkey *et al.*, 1980; Droxler & Schlager, 1985; Schlager *et al.*, 1994; Page & Dickens, 2005; Jorry *et al.*, 2010). Pilkey *et al.* (1980) found that thin, but frequent and basin-wide turbidites and debris flow layers are common in active margin basins such as the Hispaniola-Caico and Navidad basins. In tectonically quiet carbonate platform, adjacent basins such as the Columbus, Tongue of the Ocean and Exhuma basins, discontinuous, but thick sand-rich layers are more common due to numerous entry points and extensive source areas. Climate control on carbonate deposition is most often discussed in terms of the platforms response to sea-level change and the prevailing oceanographic conditions (e.g. windward vs. leeward effects, Mullins & Neumann, 1979). Increased sediment dispersal into carbonate platform and reef-adjacent basins during sea-level highstands (highstand shedding; Schlager *et al.*, 1994) and the opposite (lowstand shedding, e.g. Shanmugam & Moiola, 1984) have both been proposed to explain observations of time-varying sediment accumulation in these tectonically inactive regions.

The study presented here examines the shallow stratigraphy of two deep-water basins within the SW Anegada Passage in the NE Caribbean, the Virgin Islands (VIB) and Whiting (WB) basins (Fig. 1), to determine the recent history of sediment transport events in the region. The NE Caribbean, in which these basins are located, is a tectonically complex and seismically active region that is also frequented by hurricanes. These powerful processes may provide the necessary triggering to initiate sediment transport to the basin floors and in the case of earthquakes, cause internal deformation of layers deposited on the basin floors (seismites). Damaging earthquakes have occurred in the Anegada Passage region numerous times over the last few centuries (Robson, 1964; McCann, 1985;

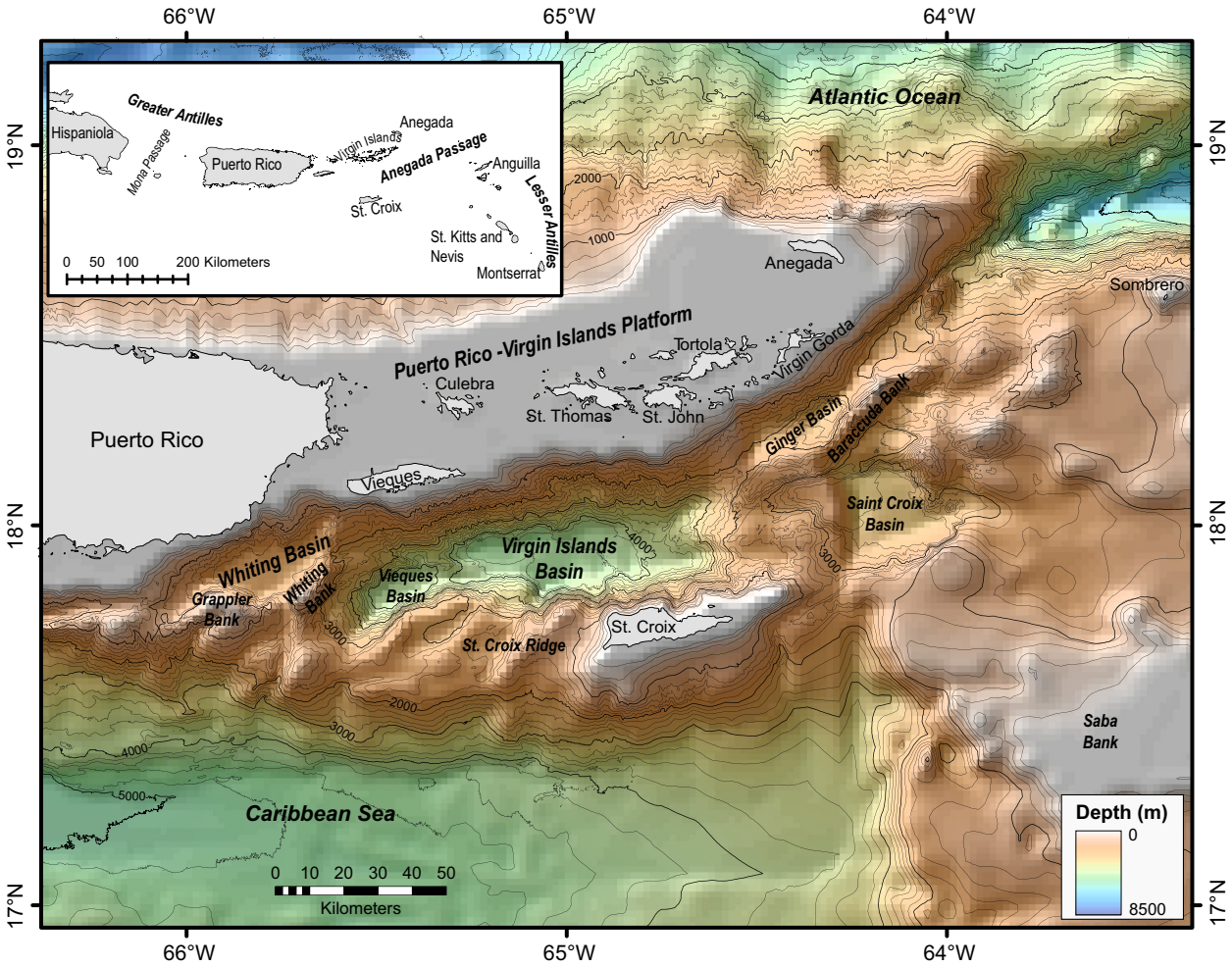

Fig. 1. Anegada Passage region, northeast Caribbean. The Anegada Passage is located at the intersection of the Greater and Lesser Antilles (inset), between the Virgin Islands and Anegada to the north and St. Croix and Anguilla to the south. Colour bathymetry is derived from the ETOPO1 data set (Amante & Eakins, 2009). Contour interval is 200 m.

ten Brink *et al.*, 2011) and historical and geological records of significant Atlantic hurricanes and tropical storms that pass through the region are extensive. At least 45 hurricanes with recorded onshore damage have impacted the region since 1529 (Boose *et al.*, 2004; García-Herrera *et al.*, 2005), with geological evidence of intense hurricane activity (Donnelly & Woodruff, 2007) reaching back as far as 5000 years. These storms are capable of initiating significant sediment transport on the shallow shelves surrounding the Virgin Islands and Puerto Rico (Hubbard, 1992; Donnelly, 2005). Recent studies (e.g. López-Venegas *et al.*, 2008) have further shown that failure of submarine slopes along the NE Caribbean plate boundary is a potential sources of tsunamis in the region. The earthquake and tsunami of 18 November 1867, whose source region was likely in the Anegada Passage (Reid & Taber, 1920; Barkan & ten Brink, 2010), caused extensive damage to settlements throughout the NE Caribbean, especially those on the Virgin Islands.

GEOLOGICAL SETTING

The Anegada Passage is a deep-water basin and ridge province separating the islands of the Puerto Rico-Virgin Islands (PR-VI) platform from the islands of St. Croix and Anguilla (Fig. 1). Ridges in the passage are often steep sided, reaching depths as shallow as 40 mbsl (metres below sea level). The maximum depth in the passage is in the VIB at 4530 mbsl. The Anegada Passage is the only pathway for entry of North Atlantic Deep Water (NADW) into the Caribbean Sea (Fratantoni *et al.*, 1997; Johns *et al.*, 2002).

The deformation history and ongoing tectonic activity of the NE Caribbean continue to be matters of considerable debate (e.g. Speed, 1989; Jany *et al.*, 1990; van Gestel *et al.*, 1998; Raussen *et al.*, 2013). Sinistral and dextral transtensional deformation models, often including microplate rotation, have been proposed to explain the development of the Anegada Passage and the VIB in particular. Jany *et al.* (1990) concluded that the St. Croix Basin and VIB are pull-apart basins created within a dextral strike-slip environment, possibly subsequent to an earlier phase of sinistral deformation. In this model, the WB, Vieques Basin and VIB are bound by normal faults (represented by the steep basin walls) and minor dextral strike-slip faults, with a major NE–SW-trending dextral strike-slip fault located within the NE section of the Anegada Passage. Gill *et al.* (1999) propose a sinistral transtensional deformation model for the region, based on structural, morphological, and sedimentary evidence from St. Croix and the surrounding normal fault-bound basins; an interpretation recently supported by Raussen *et al.* (2013). Global Positioning System (GPS) data show the islands of Vieques, Culebra and St. Thomas (Fig. 1) moving to the NW relative to St. Croix at a rate of 1–1.5 mm year^{-1} (ten Brink & Lopez-Venegas, 2012), supporting the Gill *et al.* (1999) model.

The composite geology of Puerto Rico and the Virgin Islands is a reflection of an evolving island arc terrane underlain to varying degrees by subducted North American Plate oceanic lithosphere and capped by a stable carbonate platform (Larue, 1994). Broadly, Puerto Rico is composed of Jurassic to Eocene volcanic, volcanoclastic, and other sedimentary strata (Jolly *et al.*, 1998; Schellekens, 1998), intruded by Late Cretaceous and Eocene felsic plutons, that where overlain by Oligocene to Early Pliocene volcanoclatic and carbonate units (Larue *et al.*, 1998). Rocks on the islands of Culebra and Vieques (Fig. 1) show affinities with rocks found in northeastern and central Puerto Rico and have therefore been considered an extension of those terranes (Larue *et al.*, 1991). A sequence of Cretaceous to mid-Eocene rocks, intruded by mid- to Late-Oligocene age plutonic bodies, comprises the northern Virgin Islands (St. John, St. Thomas, Virgin Gorda, and Tortola). The island of St. Croix sits atop the elongated, NE–SW-trending St. Croix Ridge, separated from the PR-VI platform by the VIB. The island is composed primarily of highly deformed Late Cretaceous submarine fan facies, volcanoclastic turbidites and other sediment gravity flows, and mudstones (siliceous pelagic deposits; Speed & Joyce, 1989), overlain unconformably by Oligocene–Miocene mudstones and limestones (Whetten, 1966; Larue, 1994). Outcrops along the south wall of the VIB, at a depth of 3100 mbsl, have similar lithologies as the Cretaceous age formations exposed on St. Croix (Hubbard *et al.*, 1982).

The PR-VI carbonate platform is an Oligocene to Recent sequence of terrestrial and shallow marine sandstones, mudstones and limestone (reef) units which extends from Hispaniola to Anegada (Fig. 1). Southeast of Puerto Rico and south of the Virgin Islands, the PR-VI carbonate platform is approximately horizontal with average water depths <50 m and is currently mantled by extensive mesophotic reef systems. These reefs were likely re-established when the bank top was reflooded following the Last Glacial Maximum (LGM) (Smith *et al.*, 2010). The relationship of the mid- to late-Miocene limestone units of the St. Croix Ridge (Kingshill Limestone) and the limestone units of the PR-VI carbonate platform still remain unclear. Gill *et al.* (1999) suggests that Puerto Rico and the PR-VI carbonate platform may have been a source of the sediments that comprise the limestones on the St. Croix Ridge and therefore the ridge and the PR-VI carbonate platform may have been attached as late as the Miocene. Following the sea-level lowstand at the LGM, modern reef development was re-established adjacent to St. Croix *ca*. 11 ka (Hubbard *et al.*, 2005) and now encircles the island as a narrow shelf. Modern sedimentation and transport on the PR-VI platform adjacent to the basins is primarily off-bank (leeward), controlled by winds and waves that predominantly approach the area from the northeast and east (Hubbard, 1986) and by tidal currents that sweep through the shallow Vieques and Virgin Island passages.

MATERIALS AND METHODS

Bathymetry and seismic reflection data

Bathymetry coverage (50–150 m grid-cell resolution) within the study region (Fig. 2) is derived from a compilation of deep- and shallow-water multibeam bathymetry, hydrographic soundings, and shallow-water LIDAR surveys. Deep-water multibeam data were collected by the University of Madrid using the Kongsberg Simrad EM-120 on the R/V *Hesperides* in 2005 and by the U.S. Geological Survey (USGS) using the SeaBeam 2112 on the National Oceanic and Atmospheric Administration (NOAA) Ship *Ronald H. Brown* in 2006. Shallow-water multibeam surveys along the shelf and upper basin walls near St. Croix and south of the northern Virgin Islands were carried out by the NOAA Biogeography Program aboard the NOAA Ship *Nancy Foster* between 2007 and 2011. LIDAR data south of Vieques and Culebra were acquired by the U.S. Army Corps of Engineers in 2000 (JALBTCX, 2001). The NOAA Coastal Relief Model (National Geophysical Data Center, 2006) was used to fill gaps in the multibeam coverage.

Seismic reflection survey coverage across the Anegada Passage is spatially limited and of variable quality, but available lines provide valuable insight into sedimentation patterns in the deep-water basins and their relationship with structural controls. Reflection profiles used here (Fig. 2) are from the 1985 Seacarib cruise (R/V *Robert Conrad*, RC2605) collected using two 80-in^3 water guns and single-channel streamer and from the 2006 USGS R/V *Pelican* cruise which utilized a 35-in^3 generator injector (GI) gun, and a 24-channel, 240-m long streamer (see Chaytor & Ten Brink, 2010 for processing details). Additional seismic profiles (96-channel streamer, GI-gun source) collected during the Danish Galathea3 cruise were made available (H. Lykke-Andersen, pers. comm., 2012; Raussen *et al.*, 2013) for interpretation of near-surface sedimentation and structural processes.

Core and grab samples

In 2008, 10 gravity cores were collected from the WB, VIB and surrounding areas (SJ8 cores; Fig. 2) by the USGS using the R/V *Seward Johnson* and the Woods Hole Oceanographic Institution (WHOI) Giant Gravity Corer. The cores were split onshore and visually described at centimetre scale prior to nondestructive testing and sub-sampling.

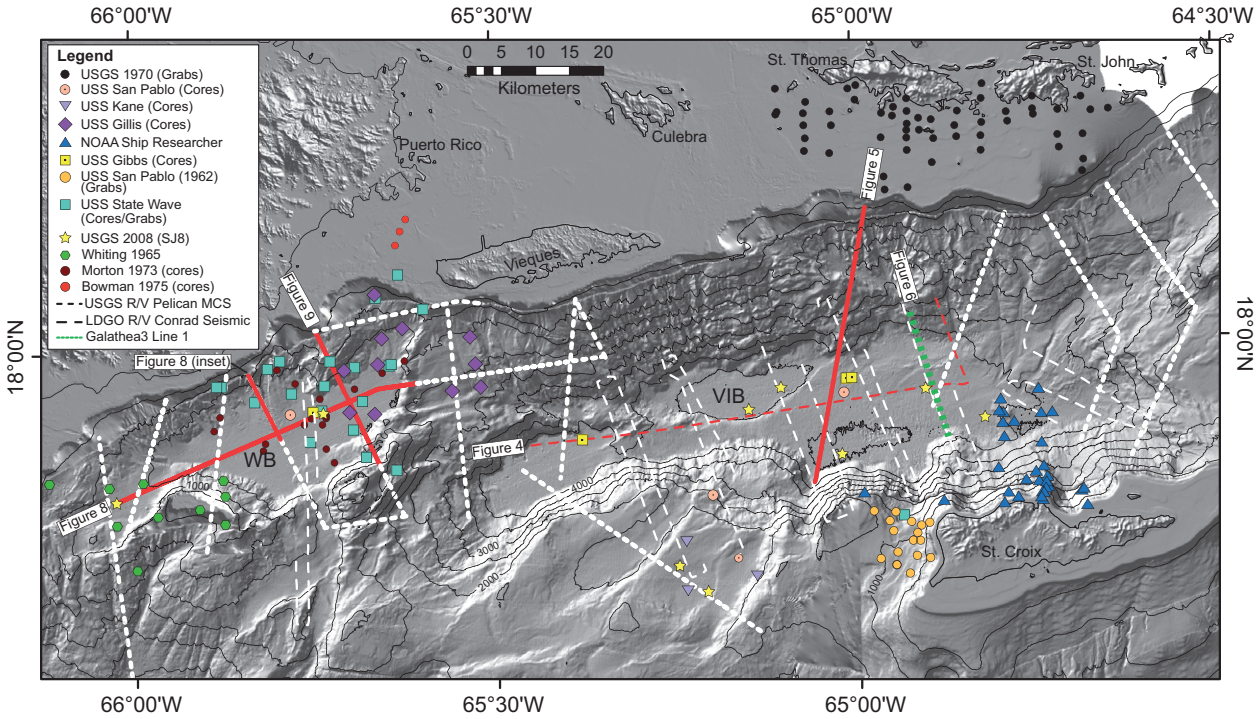

Fig. 2. Bathymetry coverage of the SE Anegada Passage, overlain with the locations of the seismic reflection and sample/core data sets used in this study. The sharp boundary between the high-resolution and low-resolution bathymetry data can be seen along the upper slope south of Puerto Rico, Vieques and the Virgin Islands and on the south and west side of St. Croix. Seismic lines, or portions of seismic lines, shown in subsequent figures are marked in red and labelled. The green-highlighted seismic line is a portion of Galethea 3 Line 1 shown in Fig. 6. Sources of core and grab samples are: USGS 1970 (Garrison *et al.*, 1971), USS San Pablo (Achstetter *et al.*, 1967b), USS Kane (Ross *et al.*, 1976), NOAA Researcher (Burton *et al.*, 1982), USS Gillis (Oser & Shumard, 1969), USS Gibbs (Achstetter *et al.*, 1967b), USS San Pablo [1962] (Ridley *et al.*, 1963), USS State Wave (Achstetter *et al.*, 1967a), Whiting 1965 (Rooney *et al.*, 1965), USGS 2008 [SJ8] (this study), Diver Samples (Bowman,1975). VIB, Virgin Islands Basin; WB, Whiting Basin. Contour interval is 500 m.

Data from pre-existing cores and grab samples from numerous sources were used to characterize the surface and sub-surface sedimentary framework of the VIB and WB (Ridley *et al.*, 1963; Rooney *et al.*, 1965; Achstetter *et al.*, 1967a,b; Oser & Shumard, 1969; Achstetter *et al.*, 1971; Garrison *et al.*, 1971; Morton, 1973; Bowman, 1975; Ross *et al.*, 1976; Burton *et al.*, 1982) (Fig. 2). In general, the cores from these sources are from the basin floors and slopes, although cores on the basin slopes are <50 cm long and therefore of limited stratigraphic value. Grab samples are from the shallower shelf regions around St. Croix, St. Thomas and St. John. Although numerous additional grab samples have been collected from the shallow shelf adjacent to Puerto Rico, and the regions surrounding the Virgin Islands, detailed grain size and composition information is lacking, requiring the use of published interpretations to describe these regions (Schneidermann *et al.*, 1976; Kindinger *et al.*, 1983).

Nondestructive testing

Physical properties were collected from the split sections of the new USGS cores using a multi-sensor core logger (MSCL) measuring gamma-ray attenuation (wet bulk density) and magnetic susceptibility at 1-cm intervals. Digital x-radiographs of each core section were acquired to highlight sedimentary structures, especially bioturbation and the fine tails of turbidites.

X-Ray Fluorescence (XRF) geochemical measurements and linescan images of selected cores were acquired at a resolution of 1 mm using an ITRAX micro-XRF scanner equipped with a 3 kW Mo target tube. The XRF scanning yields element intensities from the surface of split sediment cores providing statistically significant results (i.e. counts per second greater than 100) for K, Cl, Ca, Mn, Fe, Sr, Zr and Ar. Ratios of element counts, rather than the element counts themselves are used to overcome some of the closed-sum effects when comparing element profiles within individual cores (Lowemark *et al.*, 2010). Zirconium is assumed to be a terrigenous detrital phase sourced from the igneous bodies in Puerto Rico and the Virgin Islands and as it is unlikely to have an effect on diagenetic or biological processes; it is considered to be conservative and is used to normalize the other elements. The Ca/Fe ratio was used to identify sediment grading not observed visually (Rothwell *et al.*, 2006). Although Sr/Ca profiles have been useful in indicating the presence of shallow-water-sourced high-Sr aragonite (Rothwell *et al.*, 2006), no definitive signal was identified in data from the scanned cores.

Grain-size analysis

Sub-samples (1 cm thick) were taken at *ca*. 20-cm intervals, or more closely in sandy sediment, from selected USGS gravity cores for grain-size analysis. Grain-size data were obtained using the procedures outlined in Poppe *et al.* (2005). Additional sub-samples (each 1.5–2 cm thick) were taken above or below turbidite and other event intervals and following grain-size analyses, their coarse fractions (>63 μm) were examined for planktonic foraminifera.

Accelerator mass spectrometry (AMS) ^{14}C dating

Surface and near-surface dwelling planktonic foraminifera [*Globigerinoides ruber* (white), *Globigerinoides sacculifer* and *Globigerinella aequilateralis*] were analysed at the National Ocean Sciences Accelerator Mass Spectrometry (NOSAMS) facility. Radiocarbon ages were converted to calibrated ages using Calib 6.0 (Stuiver & Reimer, 1993) utilizing the IntCal 09 calibration curves (Reimer *et al.*, 2009) and include the generally accepted 400-year global average reservoir correction. Calibrated ages are reported as years before present (BP). Due to limited information on local marine reservoir effects and the likelihood that any local reservoir correction (ΔR) for Caribbean waters would be minimal (Hughen *et al.*, 1996; Fitzpatrick *et al.*, 2004), no ΔR value was applied during age calibrations.

RESULTS

Basin morphology and structure

Virgin Islands (VIB)/Vieques Basin

The floor of the VIB (Fig. 3) covers an area of *ca*. 890 km^2 and comprises a main basin plain, two smaller sub-basins, and a base of slope fan in the eastern portion. Seismic reflection profiles (Figs 4–6) show that the basin contains parallel to sub-parallel layered sediments over 1 km thick, which, except for the upper 150–200 m, are tilted towards the south. Tilting of the sediments likely reflects past movements along the normal faults within and adjacent to the basin (Figs 5 and 6). The basin floor outside of the sub-basins (Fig. 3a) has a *ca*. 0.5° southward dip and a *ca*. 1° dip towards the west, a result of a significant base of slope sediment wedge/fan adjacent to an isolated high at the eastern edge of the basin. A distinct downthrown sub-basin (NW sub-basin; Fig. 3) in the NW corner of the VIB is delineated by a curvilinear fault scarp. The scarp extends SW from the base of the central north wall, becoming E–W and continuing as a prominent ridge along the northern edge of the Vieques Basin (Fig. 3a). Based on seismic reflection profiles, this scarp is classified as the surface expression of a northward-dipping normal fault. An elevated sub-basin (NE sub-basin; Fig. 3a) is bounded by a sediment-covered fault-controlled ridge (FS in Figs 3a and 6) which extends west from the base of slope fan to the basin floor scarp forming the NW sub-basin. At the resolution of the bathymetry data, the entire basin floor surface appears relatively smooth, with no obvious debris blocks or prominent debris lobes.

The extensively gullied north wall of the VIB extends from the northern PR-VI carbonate platform edge to the

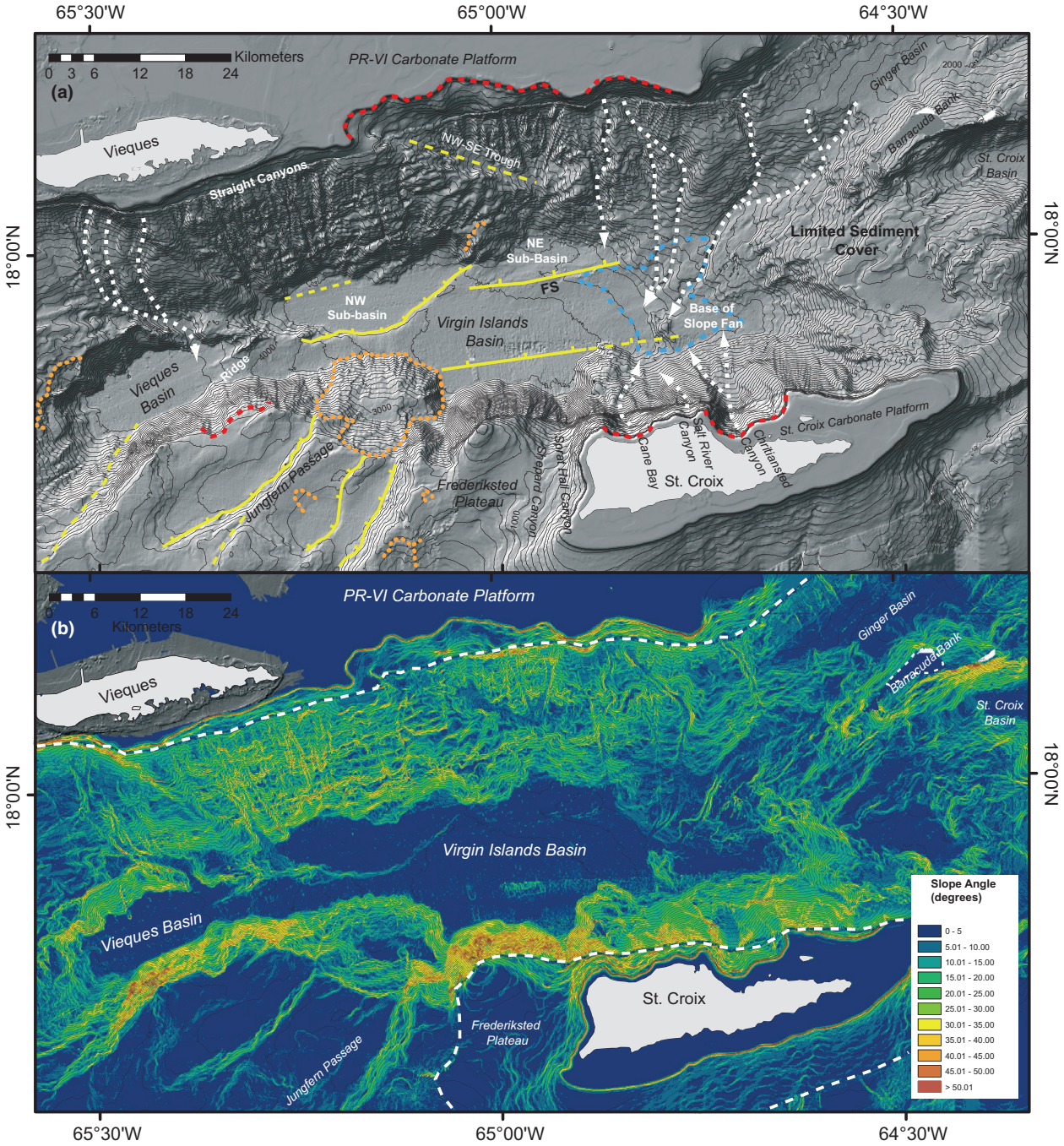

Fig. 3. (a) Bathymetry of the Virgin Islands and Vieques basins. Fault zones are marked in yellow (primarily normal motion – solid with hatching on downthrown block; possible – dashed; solid without hatching – possible transtensional fault motion). The location of the base of slope fan in the eastern Virgin Islands Basin marked by blue dashed line. Significant slope channels are marked by white dashed lines. Scalloped bank margins (red dashed lines) and possible slope failures (orange dashed lines) are highlighted. FS = Flower Structure. (b) Slope map of the Virgin Islands and Vieques basins and adjacent regions. The white dashed line marks the boundary between deeper high-resolution and shallow low-resolution bathymetry data sets. Contour interval is 100 m.

basin floor (>4000 m of vertical relief) with an average gradient of 12–14° along its western half and <10° along the eastern half (Fig. 3b). The western half of the wall is dominated by relatively straight gullies that do not appear to cut the shelf edge (Fig. 3a), but rather begin at a depth of *ca*. 600 mbsl. Available high-resolution bathymetry data between the shelf edge and the beginning of the gullies shows a smooth, convex slope that may be the result of extensive fore-reef talus deposition cut in places by what appear to be small landslide scars (NOAA Center for Coastal Monitoring & Assessment Biogeography Branch, 2012). The paths of these straight gullies are interrupted, but rarely cut or offset, at various depths by along slope ridges. At the base of the north wall, these

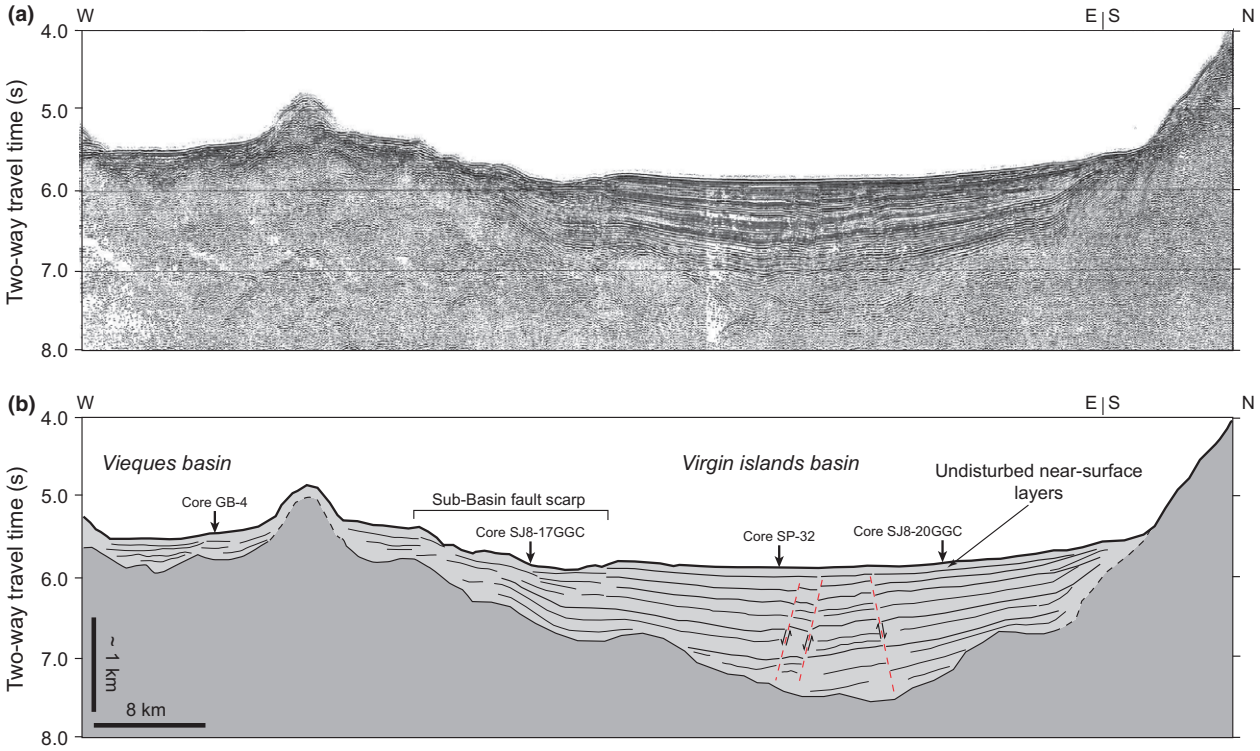

Fig. 4. (a) Uninterpreted and (b) interpreted R/V *Conrad* seismic reflection Line LDGO 122, oriented approximately W–E and then S–N, crossing the Vieques and Virgin Islands basins. Regions interpreted to be basin-fill sediments are in light grey with basement shown as dark grey. The sediments nearest the surface are undisturbed and flat lying, whereas deeper sediments appear to onlap the eastern and western edges of the basin, appear to be tilted towards the centre of the basin, and are cut by faults.

straight gullies have lower relief, with several gullies not reaching the basin floor and appearing as hanging valleys. The morphology of the eastern half of the wall is dominated by a NW–SE-oriented trough, separating drainage features of the upper wall, from hummocky terrain devoid of drainage features along the lower wall. The trough has been interpreted to be the surface expression of a fault (Jany *et al.*, 1990) which possibly ruptured during the 1867 Virgin Islands Earthquake (Barkan & ten Brink, 2010). Minor evidence of slope failure is seen near the base of the wall (Fig. 3). Further to the east, carbonate platform margin to basin floor drainage systems are re-established, although not the straight, downslope morphology as observed along the western half of the north wall. The carbonate platform edge above this part of the north wall has a number of scalloped embayments, possibly reflecting progressive escarpment erosion similar to that described in the Bahamas by Mullins & Hine (1989).

The morphology of the south wall of the VIB is markedly different from that of the north wall. The platform margin north of St. Croix has several scalloped embayments built around major submarine drainage systems. The largest embayment is *ca.* 10 km across by 4 km wide and encompasses the head of Christiansted Canyon. There are three canyons/canyon systems along the south wall of the VIB, Christiansted Canyon, Salt River Canyon, and a canyon system draining the Fredricksted Plateau, composed of Shepard, Sprat Hall and smaller unnamed canyons (Fig. 3). Christiansted and Salt River canyons have complex morphologies, with some well-defined tributary channels on the upper wall, but poorly defined or absent base of wall channels. There appears to be a well-developed fore-reef talus slope seaward of the marginal platform escarpment and modern edge reef. Gradients along the south wall of the basin are on average >20°, exceeding 40° between Christiansted Canyon and Cane Bay (except in the general location of the Salt River Canyon) and north of the Fredricksted Plateau (Fig. 3). These steep slopes have led many investigators (e.g. Shepard, 1979; Jany *et al.*, 1990) to conclude that the south wall is a normal fault scarp. West of the Fredricksted Plateau, the gradient of the south wall becomes subdued (average gradient of *ca.* 10°) coincident with the presence of a marked indent in the wall and a near horizontal bench present at a depth of *ca.* 2900 mbsl. Based on GLORIA imagery and SeaBeam bathymetry, Jany *et al.* (1990) interpreted this bench and the slope below it to be a large slump feature. Available seismic reflection profiles which cross parts of these features yield no conclusive evidence to confirm or refute a slump hypothesis. Structural control of the indent is possible due to the intersection of two major NE–SW-oriented normal faults with the south wall at its eastern and western margins (Fig. 3a).

East of the VIB is the 4195 mbsl deep Vieques Basin, separated from the VIB by a structurally controlled ridge and adjacent 50–100 m high dam of layered sediments

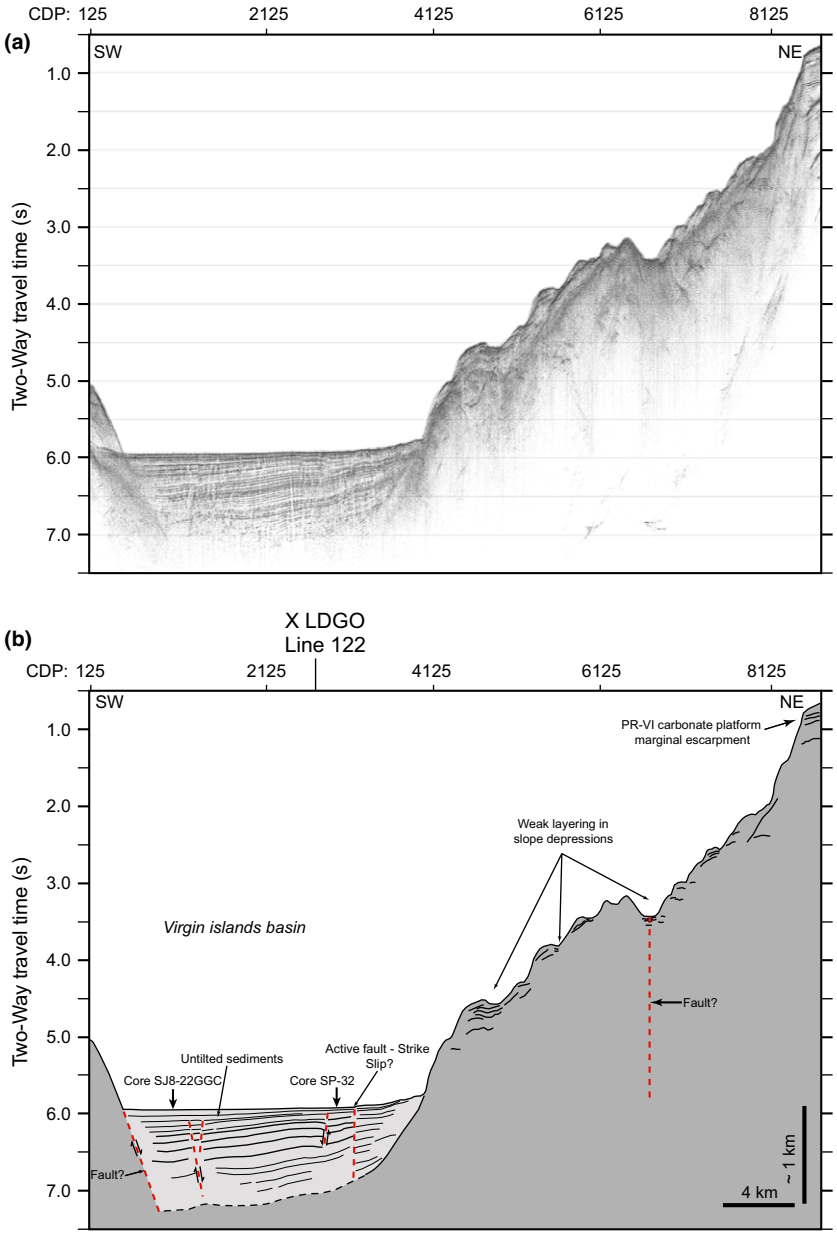

Fig. 5. (a) Uninterpreted and (b) interpreted USGS R/V *Pelican* multi-channel seismic reflection (MCS) Line 17, oriented approximately SW–NE, crossing the Virgin Islands Basin from the PR-VI carbonate platform edge to the south wall of the basin. Regions interpreted to be basin-fill sediments are in light grey with basement shown as dark grey; faults are marked by dashed red lines. Sediments nearest the surface are undisturbed and relatively flat lying, whereas those deeper are tilted towards the south and are cut by faults/fault zones. Faults may also be present at the base of the south wall and cutting the north wall. Weak layering is observed in morphological depressions on the north wall.

(Fig. 3a). A NW–SE-oriented sediment pathway that captures a number of minor canyon systems along the slope south of the island of Vieques enters the Vieques Basin adjacent to the ridge and sediment dam separating the basin from the VIB. The floor of the Vieques Basin dips towards the east at 0.02°. The steep (at times exceeding 25°; Fig. 3b) walls of the Vieques Basin display some erosional morphology, including minor scalloping of the Fredricksted Plateau along the top of the south wall. Water flow through the Jungfern Passage (Fig. 3a) outlet may be responsible for what appears to be limited sediment cover along the seafloor rimming the top of the basin walls at its western end.

The diffuse eastern margin of the VIB is a series of shallow gradient slopes, basins and ridges marking the SW end of the ridge-basin province of the NE Anegada Passage (Figs 1 and 3). The Ginger and St. Croix basins, both of which contain thick accumulations of layered sediments are perched above the VIB, separated from it by a thinly sediment-mantled, eroded bedrock slope. Numerous channels and at least one prominent landslide scar are present along the escarpment above the Ginger Basin (NOAA Center for Coastal Monitoring & Assessment Biogeography Branch, 2012). One of these channels appears to directly link the PR-VI carbonate platform to the floor of the VIB (Fig. 3).

Whiting Basin

The WB (1990 mbsl) and the adjacent shallower subsidiary Grappler sub-basin (*ca.* 1600 mbsl), are the shallowest basins in the Anegada Passage. The WB is separated from the SE coast of Puerto Rico and island of Vieques (Fig. 7) by a narrow strip of the PR-VI carbonate platform. The

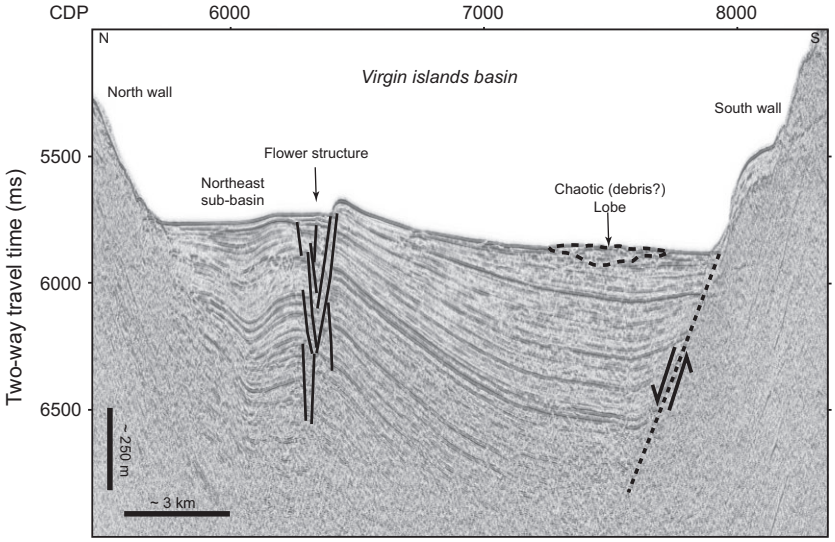

Fig. 6. Portion of Galeathea 3 MCS Line 1 (H. Lykke-Andersen, pers. comm., 2012). Line is oriented SE–NW and crosses near the eastern end of the Virgin Islands Basin (Fig. 2). A small chaotic debris deposit is observed at the base of the south wall (not visible on the bathymetry data), with deformed north-east sub-basin sediment ponded behind a generally E–W-oriented complex fault zone (flower structure, FS – Fig. 3), and the southward tilted basin sediments. Although a fault at the base of the south wall is not observed in these data, deformed basin sediments at depth along the south wall are suggestive of drag along a fault.

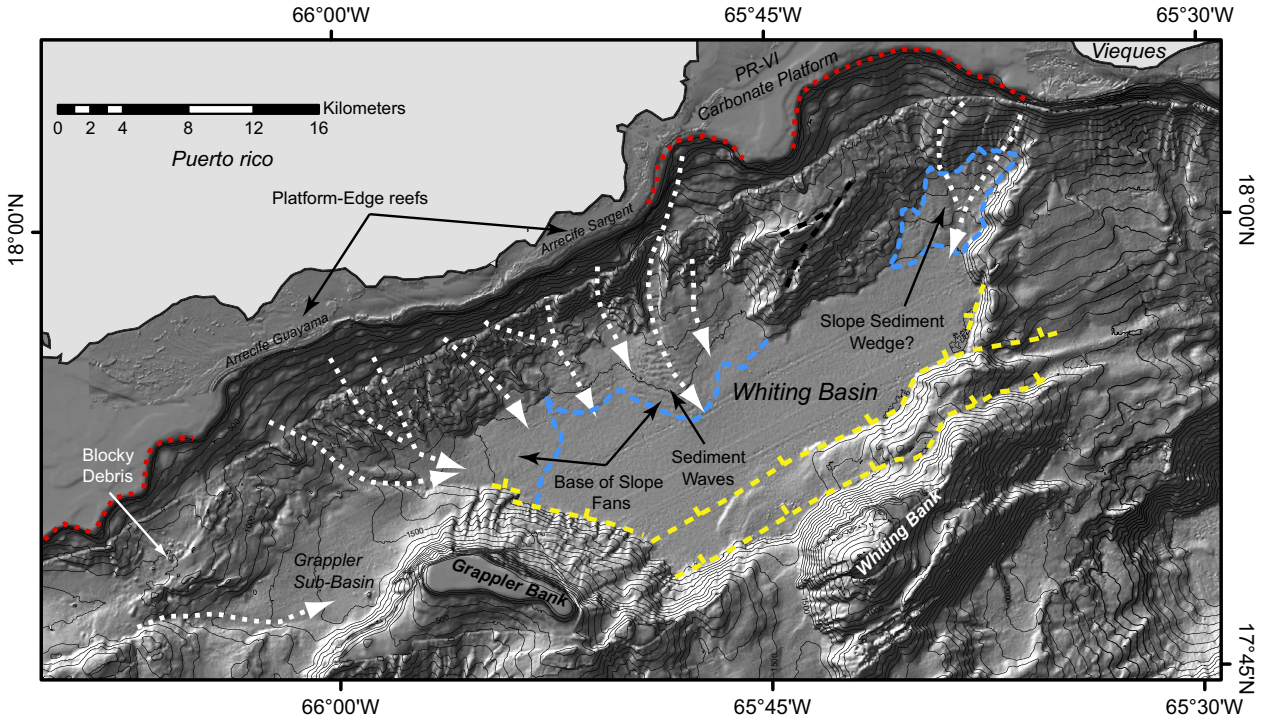

Fig. 7. (a) Bathymetry of the Whiting Basin. Fault zones visible on seismic profiles are marked by dashed yellow lines (primarily normal motion – hatching on downthrown block). The location of the base of slope fans and slope sediment wedges along the eastern and northern margins of the basin are marked by blue dashed lines. Note the presence of well-developed sediment waves on the base of slope fan along the western margin of the basin, rimmed reef margins at the edge of the carbonate platform, and the presence of debris in a slope depression above the Grappler sub-basin. Numerous slope channels are marked by white dashed lines. Scalloped bank margins and possible slope failures are highlighted by red dashed lines. Contour interval is 100 m.

southern and eastern margins of the WB are bounded by Grappler Bank – a detached remnant of the PR-VI carbonate platform, Whiting Bank and adjacent ridges slopes (Fig. 7). The gradient of the basin walls surrounding the WB vary between 10° and 50° (Fig. 7); the steepest occurring along the marginal escarpments of the PR-VI carbonate platform and Grappler Bank.

The floor of the WB (including the Grappler sub-basin) covers an area of *ca*. 260 km^2, dipping towards the SE at *ca*. 0.2°. Depositional fans have developed at the base of several slope channels along the northern wall of the basin. Sediment waves, some with amplitudes as high as 10 m and wave crest lengths up to 3.5 km, are present on the surface of the fans and in the lower reaches of the slope channels (Fig. 7). The perpendicular orientation of the wave crests to the local gradient of the fan, the appearance of the wave field only within and adjacent to slope channels, and the downslope decrease in wave amplitude and crest length are compatible with a unconfined turbidity current origin for the waves (Damuth, 1979; Nakajima

et al., 1998; Wynn *et al.*, 2000). As with the VIB, blocky debris or distinct base of slope landslide-related debris lobes are absent on the floor of the WB. A small slope basin above Grappler sub-basin appears to contain surficial debris blocks (Fig. 7). Similar to the VIB, seismic reflection profiles (Figs 8 and 9) show that the basin contains parallel to sub-parallel layered sediments over 1 km thick, interrupted by normal faults along the basin margins and by chaotic deposits, likely related to the base of slope fans (Fig. 8).

Prominent platform-edge reef banks adorn the top of the scalloped northern wall of the WB and likely play a role in controlling sediment delivery to the basin margins and floor. Slope channels are well developed along the north wall of the basin, although the majority of them have flat, partially sediment-filled floors. Two major embayments along the platform edge are located above basin floor depositional fans, suggesting that these areas are the primary locations for sediment entering the basin from the north (Fig. 8). The steep south wall of the WB is largely devoid of channelized features, except north of Grappler Bank (Grappler Seamount), which would have been sub-aerially exposed during the last glacial period. There appears to be some evidence of landslides scars along the fore-reef slope along the PR–VI carbonate platform north of the WB (NOAA Center for Coastal Monitoring & Assessment Biogeography Branch, 2012) as well as along the NE edge of Whiting Bank.

Surficial and sub-surface sediments

In this work, a generic size fraction-based classification system, rather than a depositional texture system (e.g. Dunham, 1962) is used to describe surficial and sub-surface sediments within and adjacent to the basins. This is due to limited texture information available in the older published and unpublished data sources.

Surficial sediments

The composition and texture of surficial sediments in the VIB and WB regions vary considerably from shelf to basin floor environments, and provide a valuable snap-shot of the modern sediment distribution and deposition processes in the area. Surficial sediments in the VIB show a trend of decreasing grain size and increasing pelagic contribution with increasing water depth (Fig. 10). In general, sediments present on the shallow shelves and platforms rimming the basin to the north and south are characterized by coarse-grained sands and gravels primarily composed of coral and other larger carbonate fragments (Kindinger *et al.*, 1983; Hubbard *et al.*, 1990). Sandy-silts along the upper slope (depths between 300 and 2000 mbsl) give way to clayey-silts on the lower slope (Fig. 10a), with a corresponding decrease in shallow-water carbonate constituents (Burton *et al.*, 1982). The distribution of gravel-sized components also varies considerably and appears primarily controlled by the presence of a shelf conduit (e.g. Christiansted, Salt River and Cane Bay canyons). Along the south wall of the VIB, Burton *et al.* (1982) and Hubbard *et al.* (1982) observed pebble to boulder-size rock and coral fragment debris scattered widely across the slope, but there is no evidence that these are ultimately deposited on the basin floor.

As with the VIB, surface sediments on the upper walls of the WB, especially immediately below the marginal

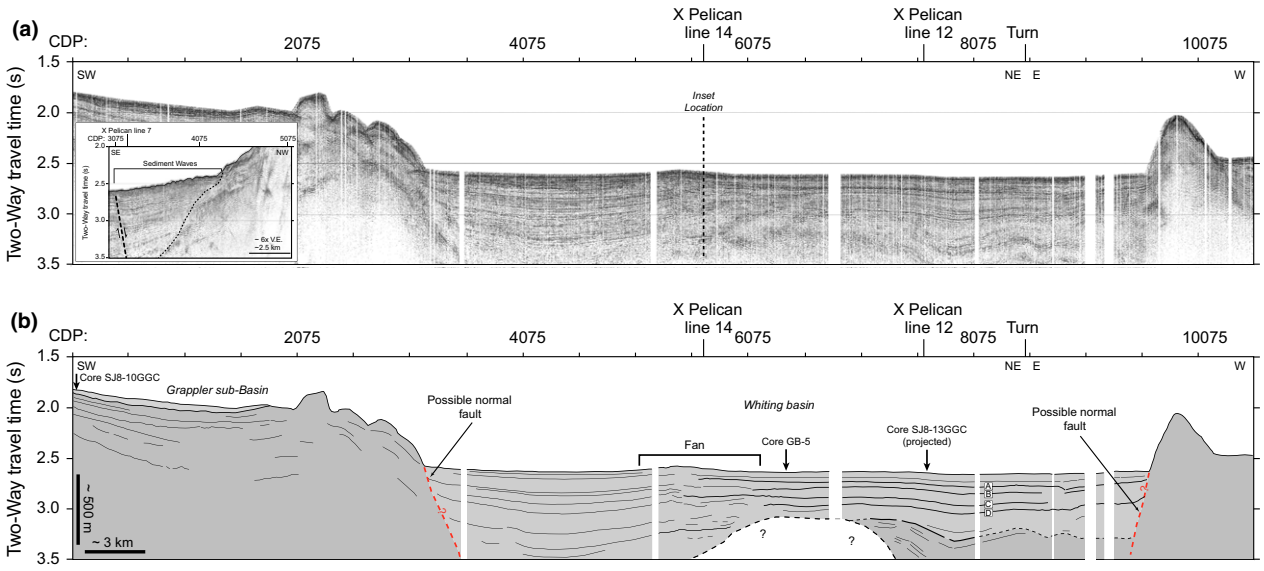

Fig. 8. (a) Uninterpreted and (b) interpreted portion of USGS R/V *Pelican* MCS Line 7 oriented SW–NE, becoming *ca.* E–W, crossing through the Whiting Basin and Grappler Sub-Basin. Submarine fan deposition is prominent within the centre of the basin, disrupting the continuity of sediment layering across the width of the basin. Normal faults may be present at the margins of the basin (see Fig. 8a). Deformed layering (dark grey) is seen below the basin sediments. Lettered horizons correlate with horizons identified in R/V *Pelican* MCS Line 12 (Fig. 9). The inset shows prominent sediment waves and chaotic horizons are the manifestation of the submarine fan developed at the base of the north wall of the Whiting Basin (R/V *Pelican* line 14).

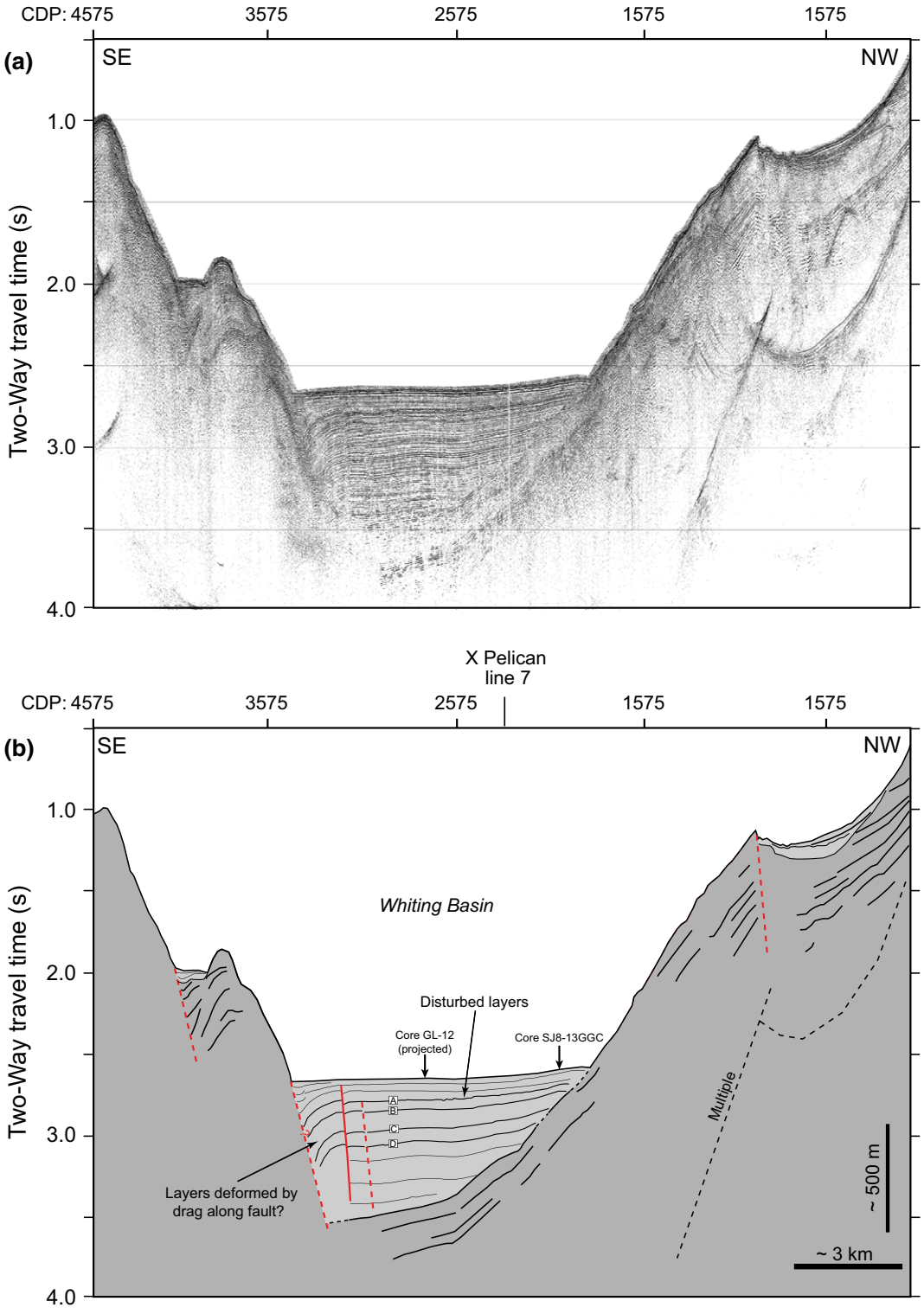

Fig. 9. (a) Uninterpreted and (b) interpreted portion of USGS R/V *Pelican* MCS Line 12 oriented SE–NW across the eastern Whiting Basin. Sediment layers (light grey) are seen to onlap the north wall of the basin, but are deformed to the south likely as a result of drag along basin margin normal faults. Tilted carbonate platform sections appear to form the bulk of the north wall of the basin, where slope depressions formed by fault movement trap sediments entering the basin. Disturbed layering (horizon A) likely reflects sediment waves, but may be the result of seismic shaking or debris flow deposition.

escarpment of the PR-VI carbonate platform and around Grappler Bank, are primarily sands and silty sands; changing to clay-rich silts on the deeper parts of the walls and basin floor (Fig. 10b). Surface sediments from shallow cores taken on the top of the PR-VI carbonate platform in the Vieques Passage are composed primarily of coarse carbonate sands, gravel-size shell fragments and plant material (Bowman, 1975). Schneidermann *et al.*

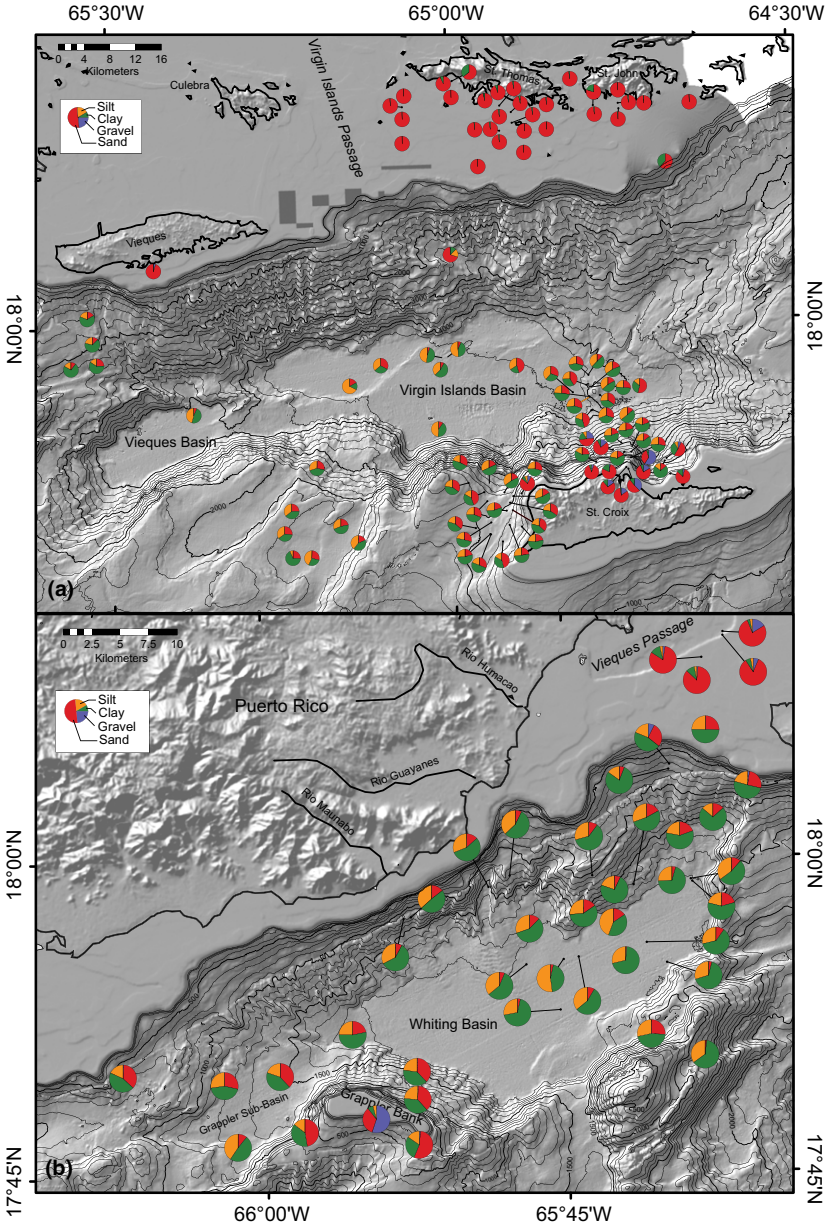

Fig. 10. Grab sample and core-top textural plots showing the variation in sediment grain sizes from the carbonate platform tops to the floors of the (a) Virgin Islands and Vieques basins and (b) Whiting Basin. Carbonate platform tops and adjacent fore-reef aprons are dominated by sand and gravel-size materials, whereas basin slopes are silt dominated. Surficial sediment of the basin floors is dominated by the clay-size fraction, but still contains a significant silt- and sand-size fraction, reflecting the presence of foraminifera and pteropod tests. Single textural sample on the north wall of the Virgin Islands Basin is from a Hercules ROV push collected in 2013 by the E/V Nautilus (ten Brink *et al.*, 2014).

(1976) found that the coarse carbonate sand–gravel mix gives way to coral fragment-dominated sand at the edge of the PR-VI carbonate platform south of Vieques and southeastern Puerto Rico where extensive coral reef systems are found.

Sub-surface sediments

Sediments within the upper few metres of the floors of the VIB and WB are in general a sequence of fine-grained pelagic carbonates and intervening layers of graded or ungraded bioclastic silts and sands. Within the VIB, a third facies was identified, characterized by a homogeneous clay-dominated interval devoid of any significant biogenic components.

Pelagic carbonates. The pelagic carbonate sediments (oozes) are primarily composed of varying quantities of planktonic foraminifera (e.g. *Globigerinella aequilateralis*, *Globigerinoides ruber, Globigerinoides sacculifer, Orbulina universa*, *Neogloboquadrina dutertrei*, *Globorotalia menardii and Globorotalia tumida*), thecosome pteropods (*Diacria* and *Cresis* sp.), sponge spicules (porifera) and fine shell debris within a carbonate-rich clay and silt matrix. Small gastropod shells, igneous rock fragments and quartz grains are often found as minor constituents within the pelagic layers. Analysis of the clay fraction was not carried out, but Babcock (1970) identified kaolinite as the dominant clay mineral in pelagic layers of the WB. The carbonate content of these layers varies between 60% and 92% (Achstetter *et al.*, 1967a, 1971; Morton, 1973; Burton *et al.*, 1982).

Foraminifera tests show negligible recrystallization, degradation or overgrowth, likely due to the regional calcium compensation depth in nearby Atlantic waters, which are entering the Caribbean via the Anegada Pas-

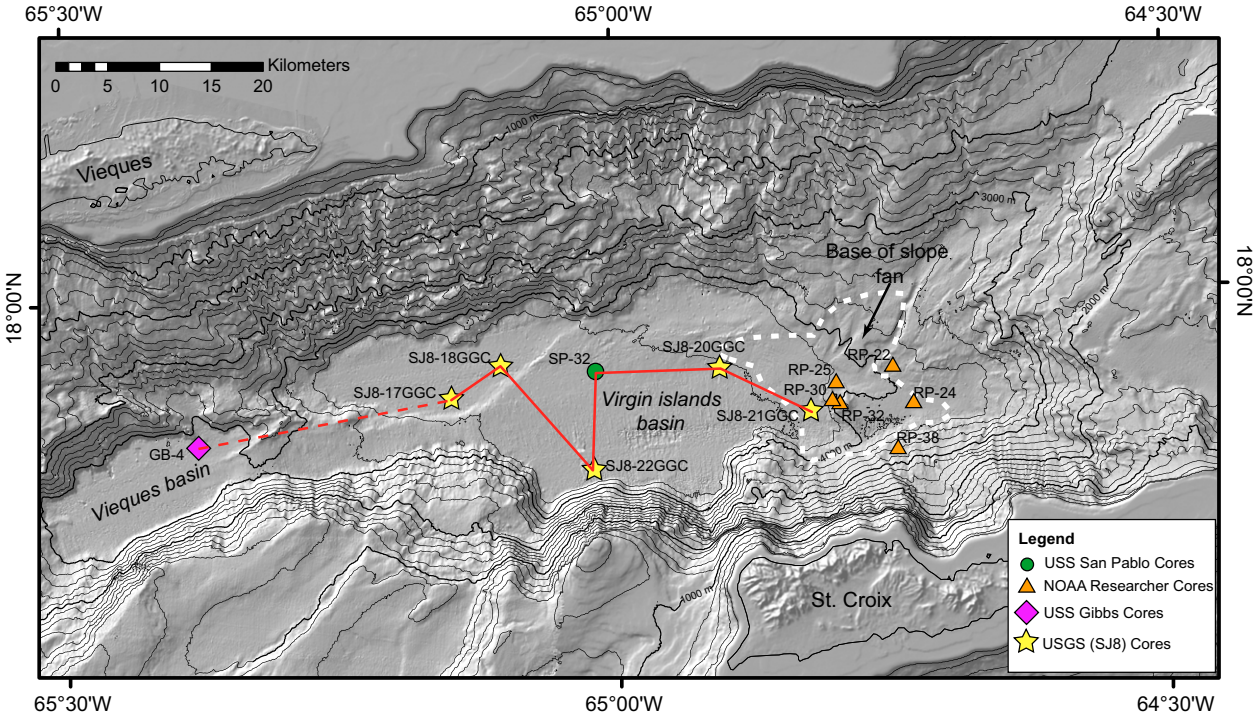

Fig. 11. Map of core sites in the Virgin Islands and Vieques basins used to investigate the near-surface sediment distribution. The red line marks the location of sites used for site correlation as shown in Fig. 16. Contour interval is 200 m.

sage, being at *ca*. 6000 mbsl (Biscaye *et al.*, 1976). The aragonite compensation depth is at *ca*. 3800 mbsl in this region (Gerhardt & Henrich, 2001), which is significantly shallower than the floor of the VIB. Aragonite pteropod tests in the pelagic layers in cores from both the VIB and WB show little to no visible evidence of chemical abrasion or recrystallization, but the vast majority of the tests are broken, which is thought to be a result of dissolution processes (Almogi-labin *et al.*, 1986; Droxler *et al.*, 1988; Haddad & Droxler, 1996). Mottling is apparent on x-radiographs throughout many of the pelagic units suggesting bioturbation, but well-defined burrows were not always observed. A colour transition from pale- or yellow-brown to grey, grey-green or white pelagic mud occurs within the upper 30 cm in most cores from both the VIB and WB. Such colour shifts in sediments from the Tongue of the Ocean where attributed by Schlager & Chermak (1979) to be the result of a change in carbonate content resulting from sea-level lowstand (white) to highstand (green) conditions. Alternatively, these colour changes may merely represent digenetic changes in redox conditions (Morton, 1975; Lyle, 1983).

Grain-size analyses show that the pelagic layers are very poorly sorted (standard deviation [SD] >2), with a mean size generally >6.5 phi (fine silt). Foraminifera and pteropod tests constitute the primary source of material in the sand and silt-sized fraction. In core SJ8-21GGC at the eastern part of the VIB (Fig. 11), layers that appear to be pelagic in origin tend to be sandier due to the increase concentration of igneous rock and carbonate rock fragments, possibly signalling that they are the tails of turbidites. No significant variation in the composition of the pelagic carbonate layers was noted between the VIB and WB, suggesting that this facies represents background sedimentation that blankets the entire Anegada Passage region.

Turbidites/sandy debris flows

Compositionally, sand layers [defined for the purposes of this study as one in which the sand fraction (0.062–2 mm; 4 to −1 phi) is by weight the dominant component] contain a mix of planktonic foraminifera and pteropod tests, igneous rock fragments, mica, quartz grains, carbonate fragments, spicules, and broken shell and skeletal debris. In addition, a number of sand layers in both the VIB and WB contain a significant amount of shallow-water (neritic) components, such as coral fragments, bryzoans, gastropods and coralline algae (e.g. *Halimeda* plates). Two pieces of pumice, one *ca*. 1-cm long, where found within a 1 cm-thick sand layer in core SJ8-20GGC (Fig. 11). As no local source of pumice is present in the Puerto Rico-Virgin Islands region, a most likely source for this material is one of the volcanic islands of the Lesser Antilles.

Other than the pumice fragments, no significant gravel-size (>−1 phi) fraction was present in any sand layer and in fact, sand layers with size factions >2 phi are only found in the eastern portion of the VIB. The thicknesses of distinct sand layers vary from <1 cm to as much as 25 cm.

The bases of these sand layers are almost always well defined and are often irregular, suggestive of some erosion. Several of the sand layers in both the VIB and WB

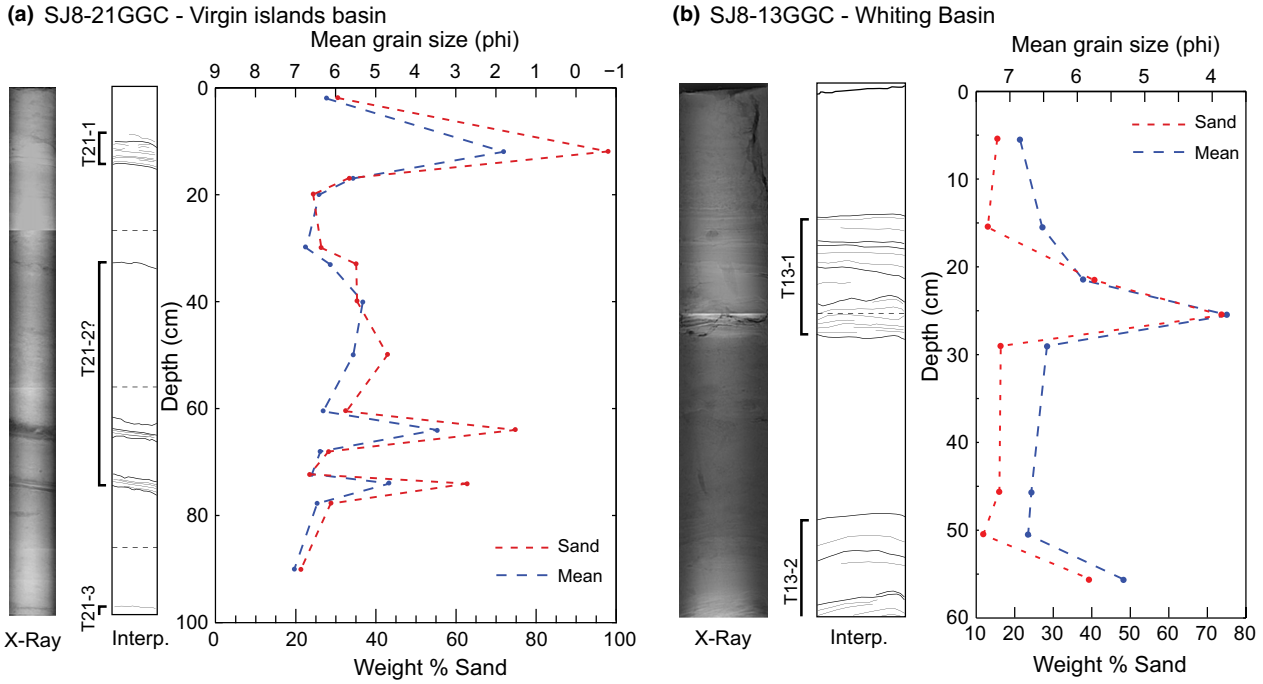

Fig. 12. X-radiograph, interpretation, and grain size/sand plots of turbidite layers from gravity cores SJ8-21GGC (a) and SJ8-13GGC (b) from the Virgin Islands and Whiting basins respectively. Dashed lines on the interpretation plots represent the edges of overlapping x-radiographs. Location of cores shown in Figs 13 and 16.

display a normally graded, moderately to poorly sorted sand fraction fining to silt and clay sizes with gradational upper contacts which are often visually indistinct from the overlying pelagic sediment. These fining-upward sequences are characteristic of deposition from turbidity currents and similar to calci-turbidites seen in other basins adjacent to carbonate banks (Jorry *et al.*, 2010). In comparison, the ungraded sand layers are very poorly sorted, have a significant clay volume that is nearly equal to the sand volume, and lack any identifiable internal layering. These layers have the characteristics of deposits from sandy debris flows (Shanmugam, 1997).

X-radiographs, grain-size data, MSCL plots and XRF data reveal the fine-scale structure and graded nature of the turbidite layers (Figs 12 and 13). The fine-grained turbidites in cores SJ8-13GGC and SJ8-21GGC (Fig. 12; for core locations see Figs 11 and 14) are composed primarily of millimetre to centimetre-scale plane-parallel laminae from their base to upper contact (Bouma Tb; Bouma *et al.*, 1962), suggestive of deposition from a low-density turbidity current (Lowe, 1982). Normally graded trends are also seen on magnetic susceptibility profiles, and to some degree wet bulk density profiles and plots of Ca/Fe and Fe/Zr from XRF analyses (Fig. 13). The response of the turbidites on the magnetic susceptibility profiles is likely driven by the high concentration and size of igneous rock fragments in the coarser size fractions, both of which decrease towards the top of the turbidites. The high magnetic susceptibility values in the profile of SJ8-21GGC when compared to that of SJ8-13GGC may be due to a greater influence of terrigenous material incorporated in the turbidity flows within the VIB. Ca/Fe profiles, which often reflect grain-size variations (Rothwell *et al.*, 2006), appear to show fining upward trends in turbidites T13-1 and T13-2 in SJ8-13GGC, but not for the ungraded sand towards the base of the core. A similar response of Ca/Fe is not seen for the turbidites in SJ8-21GGC, but a distinct upward-decreasing trend is seen in the Fe/Zr profile for turbidite T21-3 and possibly a similar, but weaker trend between 40 and 76 cm (T21-2?, Fig. 13). As with the magnetic susceptibility, trends seen in the XRF data may be responding to the changes in concentration or composition of igneous rock fragments incorporated in the gravity flows.

Structureless clay-rich intervals

Three of the USGS collected cores (SJ8-17GGC, -18GGC and -22GGC) and an additional previously collected core (SP-32; Achstetter *et al.*, 1967b) from the VIB contain a near-homogeneous, clay-rich interval that occurs below a thin (<40 cm) cover of pelagic and sandy layers (Fig. 15). The sediment in these intervals contain <0.2% sand, has a mean grain size of between 8 and 8.5 phi, and is poorly sorted (SD between 1.40 and 1.85). Compositionally, the silt-size fraction (0.004–0.063 mm) of these sediments consists of very low amounts of carbonate rock and unidentified shell fragments, spicules (tunicate and porifera), planktonic and benthic foraminifera, pteropod fragments and rare terrigenous grains. Except for occasional isolated, thin and faint bands that may be siltier material, x-radiographs reveal no obvious internal structure or bioturbation within this interval. Density and magnetic susceptibility values and XRF

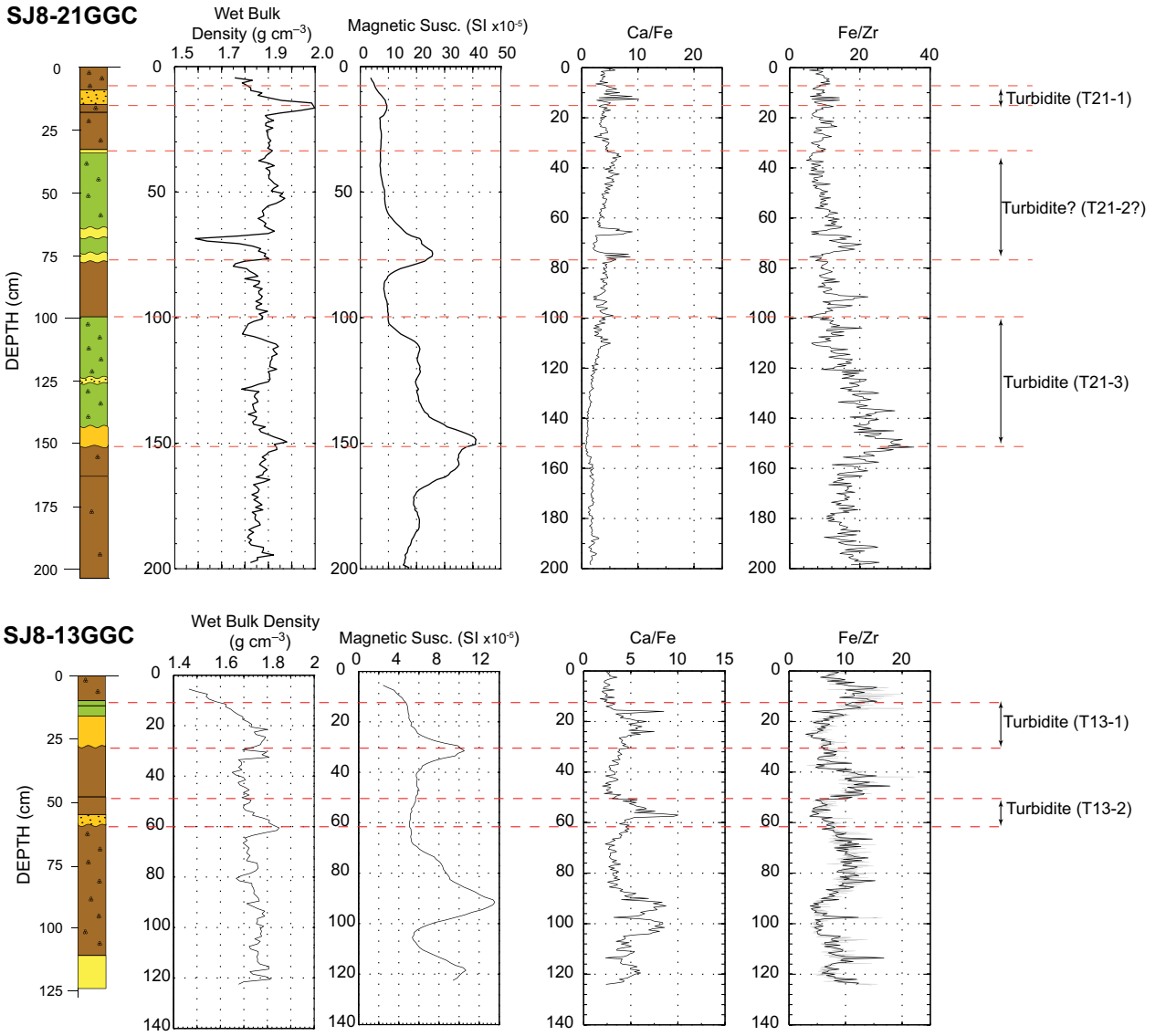

Fig. 13. Visual description (see figures 16 and 17 for description of units), wet bulk density, magnetic susceptibility and XFR ratio (Ca/Fe and Fe/Zr) plots of cores SJ8-21GGC (Virgin Islands Basin) and SJ8-13GGC (Whiting Basin) showing the down-core distribution of sandy layers and turbidites.

intensity ratios are remarkably constant down the length of this clay-rich interval in each of the scanned cores (Fig. 15). The characteristics of this interval are similar to those of unifites and homgenites, both of which are uniform mud deposits found in small, perched interslope basins (Behrens, 1984; Tripsanas *et al.*, 2004) and on the floor of some deep-water basins (Blanpied & Stanley, 1981; Kastens & Cita, 1981; Stanley, 1981). Unifite is the preferred term used to describe this facies, in part because of the similarity of the VIB to depositional environments in which unifites have been identified, but also, because it implies no specific triggering mechanism (Cita *et al.*, 1984).

Turbidite/sandy debris flow ages

To minimize sampling error, the ages of turbidites, debris flows, and other sand layers should ideally be constrained by radiocarbon dating of the pelagic intervals above and below them, taking into account bioturbation and possible erosion at the base of turbidites. Given the difficulty in consistently identifying the transition from the fine tail of turbidites to pelagic deposits due to the similar carbonate components, the bulk of the radiocarbon ages reported here were obtained from below the sand units, as close to their base as possible. As only a limited number cores were available for sampling and detailed analysis, it was not possible to establish a basis for estimating erosion at the base of these event intervals and hence ages from below the sands should be considered maximum, rather than precise, ages. Radiocarbon ages of samples from pelagic sediment above event layers were determined where it was possible to accurately identify the transition from the fine-grained tail of an event layer to the pelagic deposit, although these ages may be affected by even minimal bioturbation.

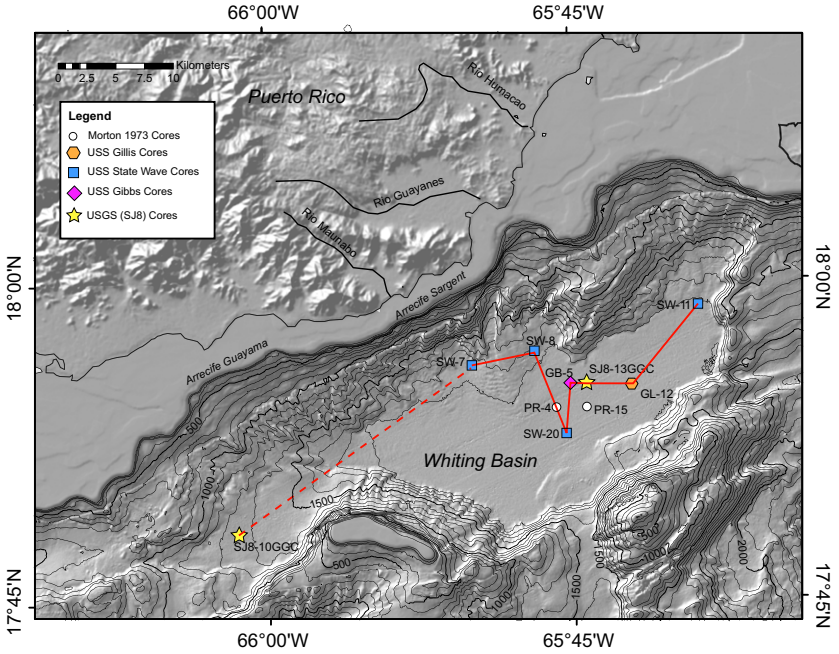

Fig. 14. Map of core sites in the Whiting Basin and sub-basin used to investigate the near-surface sediment distribution. The red line (dashed where there is a significant distance between sites) marks the location of sites used for site correlation as shown in Fig. 17. Contour interval is 200 m.

The oldest turbidite encountered in the VIB is T21-3 (SJ8-21GGC) with a maximum age of 19 156 ± 247 years BP (Table 1; Fig. 16). The absence of *G. menardii* and *Globorotalia tumida* in this interval supports a pre-Holocene age (Sexton & Norris, 2011). Ages of 15 045 ± 440 and 13 681 ± 201 years BP were obtained from below a sandy interval containing shallow-water fauna at *ca*. 125 cm in SJ8-21GGC (Fig. 16). The presence of these younger age sediments in what is interpreted to be the tail of turbidite T21-3 suggests that the generating turbidity current was erosive or that T21-3 is a subtly stacked deposit representing more than one event. Turbidite T21-2 in SJ8-21GGC and a sand layer between 63 and 64 cm in SJ8-20GGC were dated at 10 242 ± 97 and 12 877 ± 197 years respectively. The higher abundance of *G. tumida* compared to *G. menardii* in these intervals is similar to that noted by Sexton & Norris (2011) close to the *ca*. 11.5 ka (average) tropical Atlantic re-appearance datum of these two species, providing corroborating support for the validity of these dates. Turbidite T21-1 in SJ8-21GGC and thin, ungraded sandy layers in the upper 10 cm of SJ8-18GGC and SJ8-22GGC have ages showing emplacement between *ca*. 2100 and 1000 years (Table 1; Fig. 16). Pelagic sediment immediately above the unifite in core SJ8-18GGC was dated at 3217 ± 106 years.

Pelagic sediment directly below the shallowest turbidite in core SJ8-13GGC from the WB yielded an age of 2539 ± 133 years (Table 1, Fig. 17). An age of 12 698 ± 124 years was determined for pelagic sediments above a silty-sand interval at the base of SJ8-13GGC. Although the age was determined from the base of the pelagic layer directly above the basal coarser interval and therefore prone to have incorporated the fine-grained tail of a turbidite, the high abundance of *G. tumida* and near absence of *G. menardii*, are compatible with the pre-8 ka age-abundance ratios of *G. menardii* and *G. tumida* of Sexton & Norris (2011), providing some validation for the age.

Sedimentation rates

Although subject to errors, bulk (including rapidly deposited layers such as turbidites and sandy debris layers) and pelagic sedimentation rates provide a useful guide for determining the sedimentary development of a basin. The limited length and dating coverage of the cores, possible missing material from core tops, the difficulty in distinguishing the fine tail of turbidites, and determining the magnitude of erosion at the base of high-energy deposits are all potential sources of error in these calculations. In the absence of robust constraining information, we have assumed the aforementioned errors to be negligible to determine first order sedimentation rates.

Based on the 21 cm thickness of material above the unifite layer in SJ8-18GGC, the bulk sedimentation rate in the central VIB is calculated to be between 6.9 and 7.4 cm/1000 years for the last 3200 years. Removing the thin sand layer located between 1 and 3 cm, gives a pelagic sedimentation rate of 6.3–6.8 cm/1000 years. However, the 1 cm-thick layer of pelagic sediment deposited above the sand layer (maximum age of 1577 ± 98 years) would be the result of sedimentation at a rate of 0.60-0.68 cm/1000 years. For SJ8-21GGC, the accumulation of 151 cm of sediment over 19 156 ± 247 years yields a bulk sedimentation rate of 7.8–8.0 cm/1000 years, which is reduced to 6.4 cm/1000 years and 4.3–4.7 cm/1000 years for the 76–100 cm and 0–9 cm pelagic intervals respectively.

In the WB, the bulk sedimentation rate for the upper 108 cm, based on the 12 698 ± 124 year age of the oldest

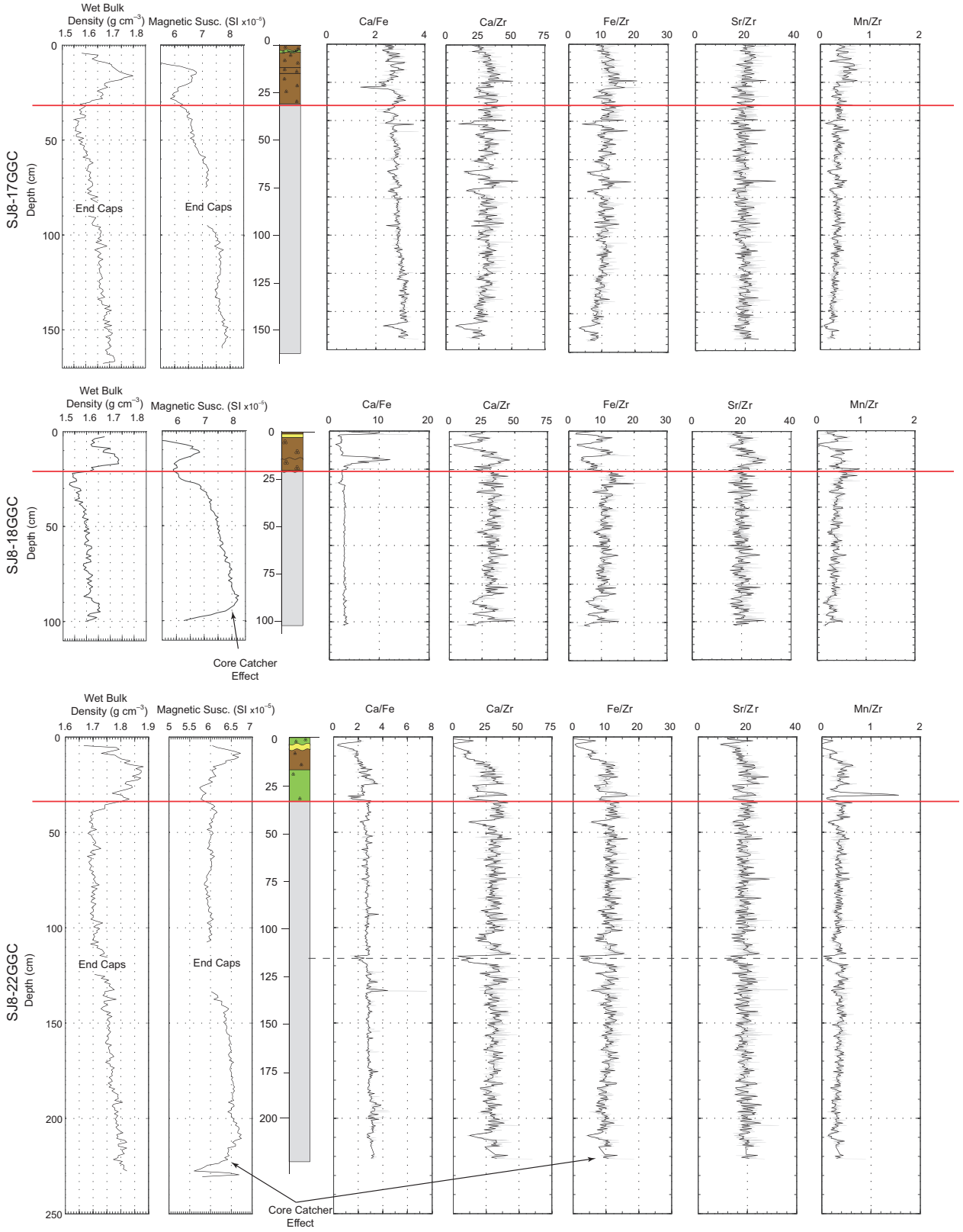

Fig. 15. Wet bulk density and magnetic susceptibility plots, visual descriptions and XRF ratio plots (light grey – unfiltered data, black line – linearly interpreted data) for gravity cores SJ8-17GGC, SJ8-18GGC and SJ8-22GGC from the Virgin Islands Basin showing the transition (red line) from pelagic interval (above) to the structureless clay (unifite) interval (below). Except for minor local variations, the MSCL and XRF ratio profiles are similar in each core. The dashed line across SJ8-22GGC marks the break between core sections.

Table 1. AMS ^{14}C radiocarbon ages and 2-σ calibrated age ranges

Core	Sample	Depth in core (cm)	Lab code	Radiocarbon age	δ13	2-σ Calibrated range (BP)	Calibrated age (BP)
SJ8-13GGC	13GGC-5	28–30	OS86530	2790 ± 25	1.26	2406–2671	2539 ± 133
	13GGC-13	108–109	OS86460	11 200 ± 40	1.21	12 574–12 822	12 698 ± 124
SJ8-18GGC	18GGC-2	3.5–5.5	OS86477	2000 ± 30	1.54	1479–1675	1577 ± 98
	18GGC-5	22–24	OS86478	3350 ± 30	1.67	3111–3322	3217 ± 106
SJ8-20GGC	20GGC-7	64–66	OS86479	11 400 ± 45	1.47	12 680–13 073	12 877 ± 197
SJ8-21GGC	21GGC-3	16–18	OS86481	2380 ± 25	1.56	1922–2101	2012 ± 90
	21GGC-14	77–78.5	OS86529	9380 ± 40	1.22	10 145–10 338	10 242 ± 97
	21GGC-19	125.5–127.5	OS86473	12 300 ± 50	1.08	13 480–13 881	13 681 ± 201
	21GGC-20	139–141	OS86533	13 100 ± 55	1.23	14 605 – 15 485	15 045 ± 440
	21GGC-22	150–152	OS86498	16 400 ± 55	0.83	18 808–19 402	19 156 ± 247
SJ8-22GGC	22GGC-1	1–2.5	OS86480	1470 ± 25	1.54	933–1094	1014 ± 81

pelagic sediment, is between 8.4 and 8.6 cm/1000 years, with a pelagic only rate (turbidites removed) of between 6.2 and 6.3 cm/1000 years. The bulk sedimentation rate over the shorter period of the last event cycle (2539 ± 133 years) is between 10.9 and 12.0 cm/1000 years, which falls to 3.7–4.2 cm/1000 years for just pelagic sedimentation. These rates vary significantly from those determined by Babcock (1970), who estimated a bulk sedimentation rate for the WB of 16 cm/1000 years and pelagic rate of 13 cm/1000 years over a period of 34 000 years. The differences in sedimentation rate estimated for the WB likely stem from the time periods over which the rates are based and the methods used for dating. We used radiocarbon dates and Babcock (1970) estimated the ages of the bases of cores from records tied to cold-warm foraminiferal transitions.

INTERVAL CORRELATIONS

Although the short length and limited spatial distribution of cores within the VIB and WB precludes detailed basin-wide interval correlations, tentative correlations are proposed as a basis for identifying sediment input pathways into the basins. Correlations are made based on sand composition (e.g. the presence of a significant shallow-water or detrital terrigenous components), age and the stratigraphic position of the layers down core.

Virgin Islands Basin correlations

A transition from dominantly pelagic and clay-rich sedimentation in the Vieques and western/central VIB to turbidite and sandy debris flow deposits in the far eastern VIB is observed in cross-hole correlations (Fig. 16). Unlike other intra-platform carbonate basins such as Exhuma Sound in the Bahamas (Crevello & Schlager, 1980) and Navidad and Hispaniola-Caicos basins (Bennetts & Pilkey, 1976; Seiglie *et al.*, 1976; Ditty *et al.*, 1977), the VIB lacks well-defined basin-wide turbidites or debris sheets within the upper few metres of the sedimentary section. Instead, these sand-rich layers are restricted to the eastern most section of the basin, where numerous channels from the north and south walls of the basin and from the Ginger Basin to the NE coalesce in a distinct base of slope fan (Fig. 3a). Therefore, it seems that at least in the recent past, coarse platform and slope material had entered the VIB by a single entry point at the eastern end of the basin, rather than via multiple entrances or line sources. Grain-size data from a number of cores within and around a high surrounded by the fan in the eastern part of the basin (location of cores shown in Fig. 13) suggest that sand layers are more abundant in the northern portion of the fan. This higher abundance is possibly a result of more gravity flows originating along the northern margin or sediment input from the Ginger Basin driven by southwestward flowing bottom currents through the Anegada Passage (Fratantoni *et al.*, 1997; Johns *et al.*, 1999).

The unifite layer is perhaps the most diagnostic and correlatable layer in the upper sedimentary layers of the basins within the SW Anegada Passage. The presence of this interval in cores at the base of the north (SJ8-17GGC and SJ8-18GGC) and south (SJ8-22GGC) walls of the VIB, as well as in a core from the central basin (SP-32), suggests that it represents a basin-wide depositional event prior to *ca*. 3.2 ka. However, it is not possible to use differential interval thickness as a guide for identifying the direction of the source of the deposit because no core has penetrated to the base of this facies.

The absence of the unifite layer from cores in the eastern portion of the basin could signal that the unifite layer is a distal deposit from a turbidity current or a deposit representing the waning phase of a debris flow which entered the basin from the east. Stanley (1981) attributes the deposition of unifites to rapid, single event deposition of fine-grained material from turbidity currents which have had their coarse-load segregated and entrapped by upper-slope basins. Sediment distribution data for the morphologically complex south wall of the VIB (Fig. 10a)

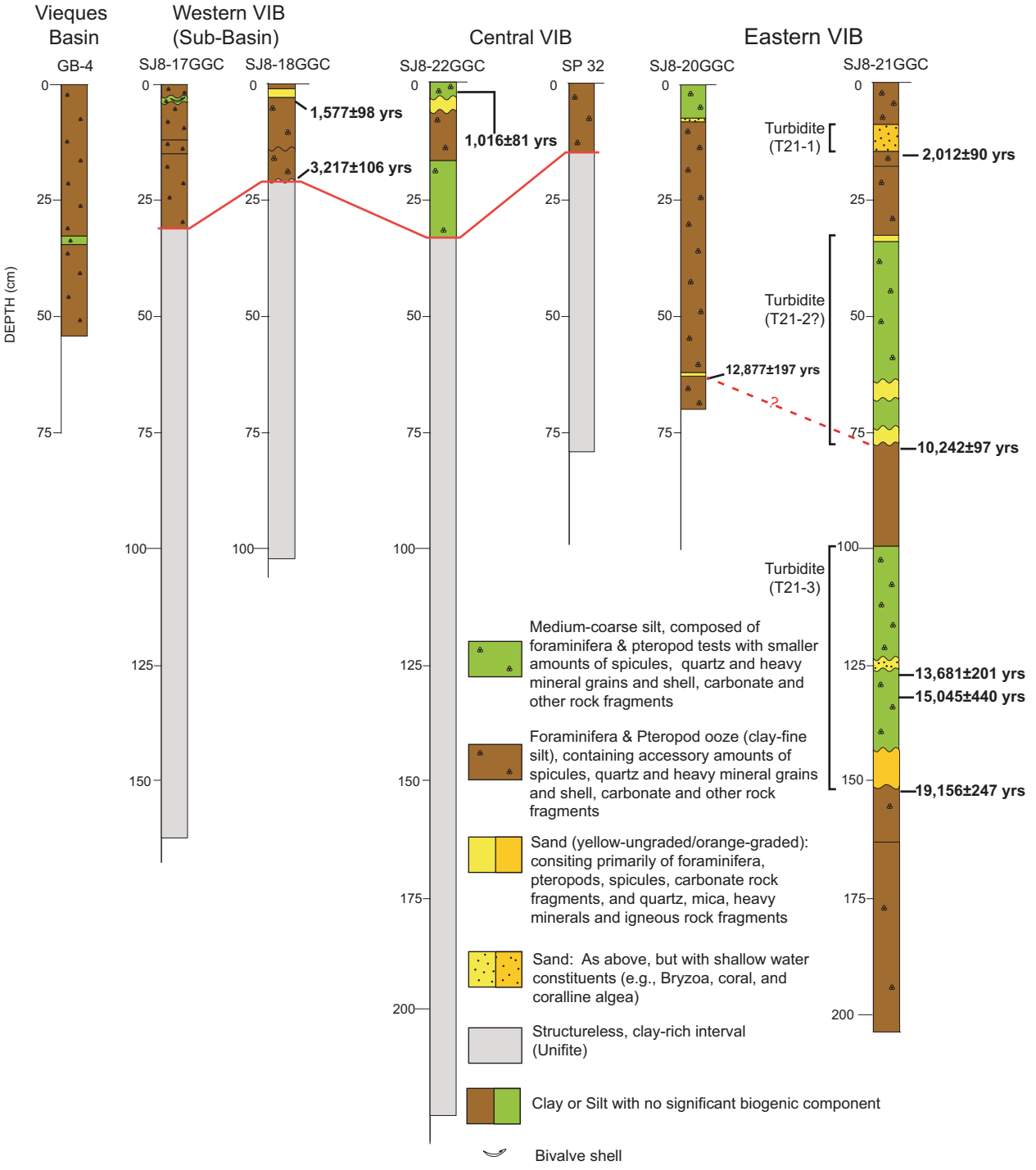

Fig. 16. Correlation plots of cores from the Virgin Islands Basin, with the calibrated radiocarbon ages (with 2-sigma errors) of pelagic sediments above or below turbidites or ungraded sand layers. Solid red line indicates the correlation of the structureless clay (unifite) layer. Dashed red lines show potential correlative layers based on down-core position and composition.

does show a downslope decrease in grain size which may reflect a progressive segregation of shelf-derived or slope-failure initiated material.

Whiting Basin correlations

Two turbidite layers are present in the upper 75 cm of three cores (GB-5, SJ8-13GGC and GL-12; Fig. 17) located in the central and eastern portions of the WB (Fig. 14). A thick, partially graded sand interval in core SW-7 at the base of a distinct slope channel along the basins west wall may correlate with the shallower of the two turbidites found in the other cores, including the turbidite in SJ8-13GGC dated at 2539 ± 133 years. A similar sand layer is not present in core SW-11 in the northeast corner of the basin,

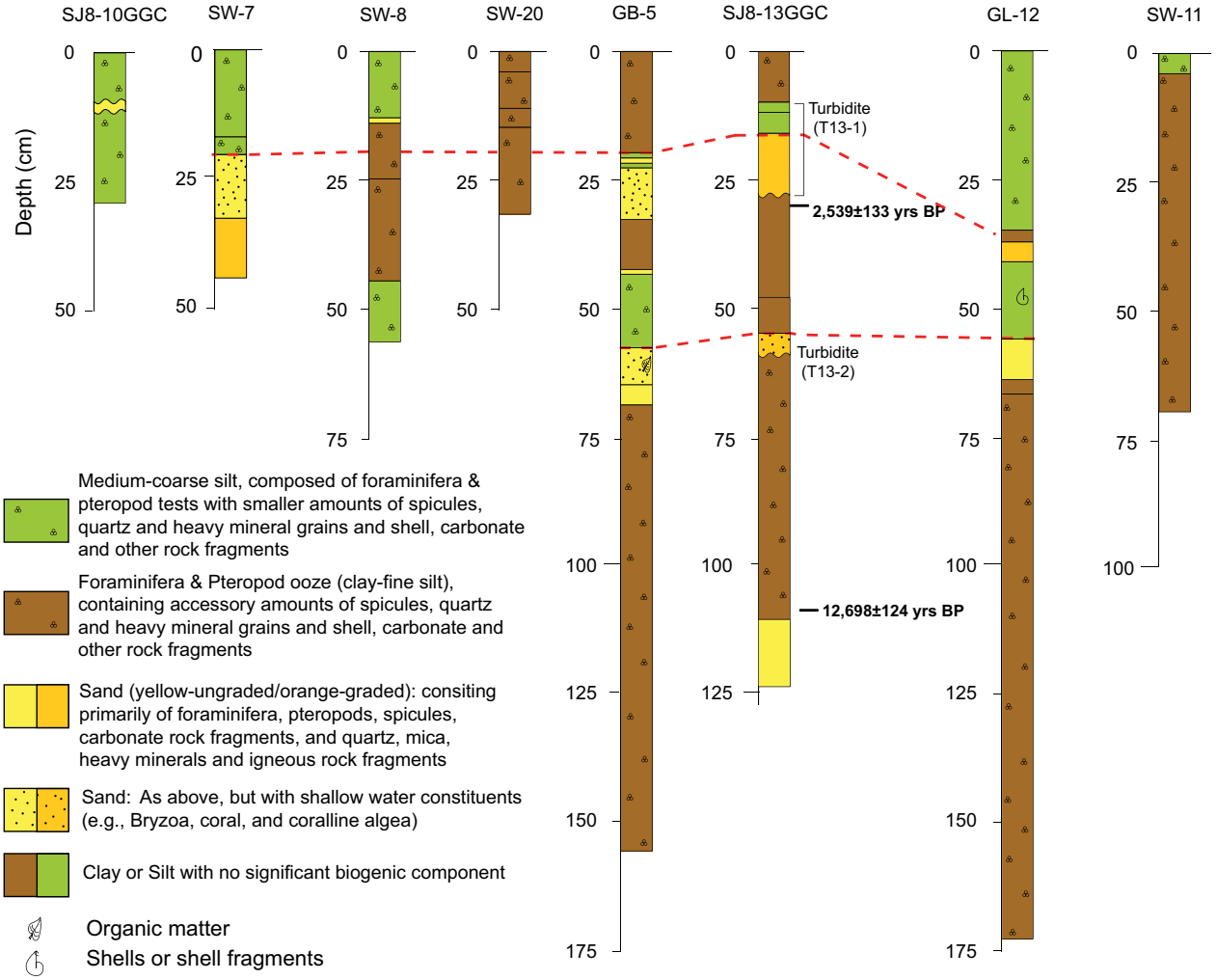

Fig. 17. Correlation plots of cores from the Whiting Basin, with the calibrated radiocarbon ages (with 2-sigma errors) of pelagic sediments above or below sand-rich intervals or turbidites. Dashed red lines show potential correlative layers based on down-core position and composition. Note the absence of sandy layers in the upper 75 cm of core SW-11 (northeast Whiting Basin), suggesting that turbidites and sandy debris flows within the cores of the central basin where sourced from a more proximal source, most likely the slope channel adjacent to SW-7 (Fig. 14).

suggesting that the source of the turbidity current was closer to the central part of the basin. Grain-size data from piston cores of Morton (1973) (Fig. 16) show the presence of another correlatable sand layer, most likely a turbidite, between 200 and 250 cm. Babcock (1970) and Morton (1973) note the presence of additional turbidites within cores taken in the WB, but detailed descriptions are not provided.

DISCUSSION

Late Quaternary sea-level fluctuations have been identified as a primary driver of the variations in neritic sediment production and shedding from carbonate bank tops into adjacent basins (Schlager *et al.*, 1994; Andresen *et al.*, 2003). Incorporated within these higher order sedimentation patterns is a depositional record from infrequent, but high magnitude climatic and tectonic events which can flush large quantities of sediment into the basins from both the carbonate bank top and basin walls. Differentiating these deposition records to extract a hurricane, earthquake, and/or tsunami record is likely to be more successful for sediments deposited in the latter part of the Holocene once the effects of slope destabilization resulting from sea-level fluctuations (Glaser, 1992; Andresen *et al.*, 2003; Jorry *et al.*, 2010) can be discounted as a primary gravity flow-initiating mechanism.

The lack of any turbidite or sandy debris flow unit within the shallow sediments of the VIB in the last *ca*. 2000 years is surprising given that triggering events, including major earthquakes and hurricanes have affected the region in recorded history. Pilkey *et al.* (1980) found that sand layer frequency increases with increasing tectonic activity, which is highlighted by the comparison between the 500 and 700 year turbidity current recurrence in the tectonically influenced Navidad Basin (Seiglie *et al.*, 1976), and the 3000–6000 year turbidity current

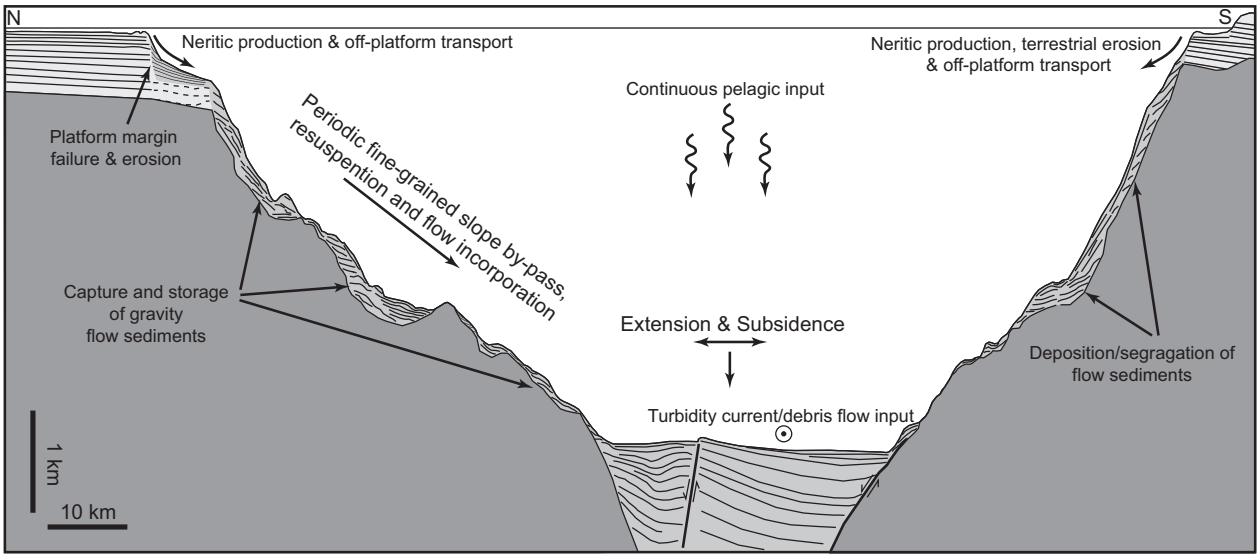

Fig. 18. Schematic illustration of the hypothesized primary production, depositional processes, and tectonic movement within the Virgin Islands Basin, highlighting the storage of sediment on the basin slopes rather than direct transport to the basin floor. Turbidity current and debris flow input are shown coming out of the page (circle with dot).

recurrence of the nontectonically influenced Columbus Basin (Bornhold & Pilkey, 1971). The *ca*. M7.2 1867 Virgin Islands earthquake likely generated ground accelerations high enough to destabilize unconsolidated material on the basin walls and initiate debris flows and turbidity currents. Furthermore, Hubbard (1992) showed that as much as 2×10^6 kg of material was exported to deep water during Hurricane Hugo in 1989. Yet, no material from these significant earthquakes and hurricanes were found in the cores. One hypothesis to explain the absence of younger event deposits in the basin floor records is that the high (*ca*. 4000 m) rugged VIB walls trap almost all the coarse material entering the basin, leading to a time-lag in, and discontinuous pattern of, deposition on the basin floor (Fig. 18). Andresen *et al.* (2003) invoked a similar hypothesis for the timing and distribution of turbidites in Walton Basin, offshore of Jamaica. Reworking and transport of these trapped sediments to the basin floor may occur during sea-level lowstands or transgressive/regressive phases. A lowstand- or transgressive/regressive-dominated shedding mechanism such as this is counter to the more commonly seen highstand-shedding process (Droxler & Schlager, 1985; Jorry *et al.*, 2010). Based on sea-level reconstructions from Barbados (Peltier & Fairbanks, 2006) and local Caribbean Sea *Acropora*-based sea-level curves (Hubbard *et al.*, 2005), flooding of the PR-VI carbonate platform most likely began *ca*. 12 ka, and *ca*. 11 ka around St. Croix. Turbidite deposition in the VIB was active possibly as much as 8000 years prior to bank top reflooding (core SJ8-21GGC; Fig. 16) signalling that highstand conditions may not have been required as a driver of sediment transport delivery to the basin floor. Sediment production and transport along the seaward edge of the PR-VI carbonate platform in the lee (south-side) of the northern Virgin Islands may also be significantly limited due to protection of platform-top reefs during both highstand and lowstand conditions. That said, the sedimentary record in the available cores for the VIB is too short to identify basin-wide variations in sediment volume, composition and deposition mechanism over the last glacial/interglacial cycle and differentiation of changes in sedimentation patterns between highstand and lowstand conditions is not well supported at this time.

Although seismic reflection profiles of the WB show widespread correlatable layers (Figs 8 and 9), the most recent turbidites appear to originate from a point source, the slope-channel system on the basins western flank, rather than multiple point- or line-source locations. The presence of neritic components and organic material within some of the turbidites suggests that the turbidity currents originated at a breach in the reef along the platform or incorporated material deposited along or just below the platform margin. The thick sequence of chaotic and stratified deposits within the base of slope fan (Fig. 8) shows that it has been a significant, if not the primary, input point of sediment to the WB for an extended period of time. As seen in the VIB, the last significant deposition event as recorded in the available cores was more than 2000 years ago, which may have been triggered by a major earthquake with a magnitude in excess of any in recorded history, or a major storm event than overloaded the accommodation space of the platform and exported a large flux of material downslope.

In addition to the low frequency of deposition of event layers within the VIB and WB, sedimentation rates in the basins may be reflective of the longer term tectonic and oceanographic development of the region and the rate at which accommodation space is made and filled. Sedimentation rates of pelagic ooze in carbonate platform environ-

ments rarely exceed 3 cm/1000 years (Rusnak & Nesteroff, 1964; Stow *et al.*, 1983), but rates as high as 40 cm/1000 years have been determined (Bornhold & Pilkey, 1971). On the other hand, bulk sedimentation rates have a wider range and are influenced by factors such as bathymetry, tectonics, sediment residence time, local and regional marine conditions, and possibly most importantly, sea level (Droxler & Schlager, 1985). In small tectonically active marginal basins, re-sedimentation of material from shallow to deep water, primarily by turbidity currents, leads to accumulation rates that vary between 0.1 and 10 m/1000 years (Stow *et al.*, 1983). In the carbonate basins of the Bahamas and Hispaniola, the addition of bioclastic turbidites to pelagic sedimentation results in accumulation rates that vary between 10 and 250 cm/1000 years (Bornhold & Pilkey, 1971; Seiglie *et al.*, 1976).

The 8.4–8.6 cm/1000 years (*ca.* 0.085 mm year^{-1}) and 6.9–7.4 cm to 7.8–8.0 cm/1000 years (*ca.* 0.07–0.08 mm year^{-1}) long-term sedimentation rates for the WB and VIB, respectively, fall within the lower end of the range of sedimentation rates calculated for basins adjacent to carbonate platforms (e.g. Bornhold & Pilkey, 1971; Seiglie *et al.*, 1976). The low sedimentation rates are influenced by the lack of gravity flow deposits and may be a combination of: (1) the ability of the high basin walls to accommodate significant quantities of sediment, (2) limited off-shelf transport and infrequent seismic or storm triggers, causing the basin to be starved of turbidity current and debris flow deposits, or (3) low rates of pelagic production and limited input of material transported by water masses entering through the Anegada Passage (Fig. 18). The somewhat higher sedimentation rates in the WB compared to the VIB are most likely the result of a greater amount of terrigenous sediment input to the shelf from Puerto Rico than is possible from the smaller Virgin Islands, and a more direct route of sediment input into the basin, leading to a greater volume of material reaching the basin floor.

The limited thickness of the basin fill (1.5–2 km) compared with the depth of the basin (up to *ca.* 4.5 km) suggests that the sedimentation rate (*ca.* 30 cm/1000 years if basin filling began at the beginning of the Pliocene) has not kept pace with subsidence (Fig. 18). As the estimated extension rate at 1–1.5 mm year^{-1} (ten Brink & Lopez-Venegas, 2012) is quite low, the present physiography of the Anegada Passage may thus be long-lived. A more specific age history cannot be determined without independent information about the subsidence rate and data-derived Neogene accumulation rates. The presence of faults that offset the VIB fill and cut its northern wall, plus the lack of stratigraphic evidence in the seismic reflection data for recent southward tilting of the basin, suggests that the basin geometry may be a relic of older tectonic regimes. This geometry has not changed significantly due to the slow rates of present tectonic activity and sedimentation. Thus, these basins are an example of a relatively old submarine relief, preserved by slow rates of tectonic activity and sedimentary processes.

CONCLUSIONS

The most recent turbidites in both the VIB and WB appear to have been deposited via point source/single basin-entry point turbidity currents, leading to the development of base of slope submarine fans. Within the VIB, a structureless clay-rich facies that is correlatable across a large portion of the basin is interpreted to be a unifite. The unifite represents either significant fine-grained slope bypass deposition, the distal deposit of a turbidite for which we did not identify the proximal deposit, or a deposit from the waning phase of an unidentified debris flow.

Recent sediment accumulation rates in the basins are very low (<10 cm/1000 years), much lower than the average for carbonate platform adjacent basins. The reasons for these low accumulation rates include limited sediment input from the carbonate platform during highstand sea-level conditions and perhaps also during lowstand conditions when the platform is exposed, sediment trapping on the high basin walls, or infrequent triggering events such as earthquakes and storms powerful enough to initiate sediment transport. The steep basin walls, in places with gradients of greater the 45°, indicate the presence of outcropping highly cohesive rock which can likely withstand high horizontal seismic accelerations. The youngest nonpelagic layers (turbidites or sandy debris layers) in the VIB and WB were deposited more than 2000 years ago, and as such, we find no evidence of sediment transport or deformation resulting from the 1867 earthquake and tsunami or recent hurricanes that have impacted the region. Furthermore, the lack of significant amount of gravel or larger-sized carbonate rock fragments in any of the available cores, suggests that submarine landslides, slumps and basin-wide blocky debris flows have not been a significant mechanism of basin margin modification in the region during the Holocene.

Basins such as those described appear to be poor recorders of past natural hazards. On the other hand, their very slow sediment accumulations rates may provide a long, condensed record of past oceanographic conditions in regions of water exchange between large ocean basins.

ACKNOWLEDGEMENTS

We thank the captains, crews, and science parties of the 2006 R/V *Pelican* and 2008 R/V *Seward Johnson* cruises for their assistance in collection of the seismic reflection data and gravity cores respectively. We appreciate the assistance with data analysis from Liviu Giosan, Kate McMullen, Heather Benway, Ethan Beise and NOSAMS. Sara Raussen, Holger Lykke-Andersen and Antoon Kuijpers, kindly shared seismic data from their Galathea3 cruise. Reviews by Homa Lee, Jack Kindinger, Jean Borgomano, Stephan Jorry, Shannon Hoy and two anonymous reviewers significantly improved this manuscript. Any use of trade, product or firm names is for

descriptive purposes only and does not imply endorsement by the U.S. Government.

REFERENCES

Achstetter, E.V., Glover, L.K., Hill, D.S., Johnson, W.R., Knoop, J.W., Ross, C.M. & Williams, V.L. (1967a) A Summary of sediment size and composition of cores and grabs for project "Aftur"; April 1967 (USS State Wave); Laboratory Item 310, U.S. Naval Oceanographic Office. Washington, DC, 59.

Achstetter, E.V., Hill, D.S. & Williams, V.L. (1967b) A summary of sound velocities, engineering properties, sediment size and composition analyses of cores and grabs for ASW/USW; (USS San Pablo); Lab Item 320, U.S. Naval Oceanographic Office. Washington, DC, 76.

Achstetter, E.V., Kelly, E.V., Kravitz, J.H., Ross, C.M. & Loomis, P.B. (1971) A summary of sediment size, composition, chemistry, x-radiography, photography, sound velocity, and engineering properties of ten cores from the caribbean and four dredge samples from the N.E. Pacific, June-October 1970 (USS Gibbs); Laboratory Item 408, U.S. Naval Oceanographic Office. Washington, DC.

Almogi-Labin, A., Luz, B. & Duplessy, J.-C. (1986) Quaternary paleo-oceanography, pteropod preservation and stable-isotope record of the Red Sea. *Palaeogeogr. Palaeoclimatol. Palaeoecol.*, **57**, 195–211.

Amante, C. & Eakins, B.W. (2009) ETOPO1 1 arc-minute global relief model: procedures, data sources and analysis. NOAA Technical Memorandum NESDIS NGDC-24, 19 pp.

Andresen, N., Reijmer, J. & Droxler, A. (2003) Timing and distribution of calciturbidites around a deeply submerged carbonate platform in a seismically active setting (Pedro Bank, Northern Nicaragua Rise, Caribbean Sea). *Int. J. Earth Sci.*, **92**, 573–592.

Babcock, L.C. (1970) Micropaleontologic correlation of a group of cores from a submarine plain southeast of Puerto Rico, naval underwater systems command. Newport, RI. TD No. 93, 10.

Barkan, R. & Ten Brink, U. (2010) Tsunami simulations of the 1867 virgin island earthquake: constraints on epicenter location and fault parameters. *Bull. Seismol. Soc. Am.*, **100**, 995–1009.

Behrens, E.W. (1984) Unifite muds in intraslope basins, northwest Gulf of Mexico. *Geo-Mar. Lett.*, **4**, 227–233.

Bennetts, K.R.W. & Pilkey, O.H. (1976) Characteristics of three turbidites, hispaniola-caicos basin. *Geol. Soc. Am. Bull.*, **87**, 1291–1300.

Biscaye, P., Kolla, V. & Turekian, K. (1976) Distribution of calcium carbonate in surface sediments of the Atlantic Ocean. *J. Geophys. Res.*, **81**, 2595–2603.

Blanpied, C. & Stanley, D.J. (1981) Uniform mud (unifite) deposition in the Hellenic Trench, eastern Mediterranean. *Smithson. Contrib. Mar. Sci.*, **13**, 40p.

Boose, E.R., Serrano, M.I. & Foster, D.R. (2004) Landscape and regional impacts of hurricanes in Puerto Rico. *Ecol. Monogr.*, **74**, 335–352.

Bornhold, B.D. & Pilkey, O.H. (1971) Bioclastic turbidite sedimentation in Columbus basin, Bahamas. *Geol. Soc. Am. Bull.*, **82**, 1341–1354.

Bouma, A.H., Kuenen, P. & Shepard, F.P. (1962) *Sedimentology of Some Flysch Deposits: A Graphic Approach to Facies Interpretation*. Elsevier, Amsterdam.

Bowman, J. (1975) A summary of sediment size and chemistry of six cores from Puerto Rico, navy divers, June 1975; Laboratory Item 488, U.S. Naval Oceanographic Office. Washington, DC, 11.

Burton, W., Bowles, F., Egloff, J., Bennett, R. & Lambert, D. (1982) Seafloor environments north St. Croix margin and Virgin Islands trough. Part 1. Introduction. Part 2. Geology and geophysics. Part 3. Geotechnical investigations. Part 4. Engineering significance, Naval Ocean Research and Development Activity, MS.

Chaytor, J.D. & Ten Brink, U.S. (2010) Extension in mona passage, northeast Caribbean. *Tectonophysics*, **493**, 74–92.

Cita, M.B., Camerlenghi, A., Kastens, K. & McCoy, F. (1984) New findings of Bronze Age homogenites in the Ionian Sea: geodynamic implications for the Mediterranean. *Mar. Geol.*, **55**, 47–62.

Crevello, P.D. & Schlager, W. (1980) Carbonate debris sheets and turbidites, Exuma Sound, Bahamas. *J. Sediment. Res.*, **50**, 1121–1147.

Damuth, J.E. (1979) Migrating sediment waves created by turbidity currents in the northern South China Basin. *Geology*, **7**, 520–523.

Ditty, P.S., Harmon, C.J., Pilkey, O.H., Ball, M.M. & Richardson, E.S. (1977) Mixed terrigenous-Carbonate sedimentation in the Hispaniola-Caicos turbidite basin. *Mar. Geol.*, **24**, 1–20.

Donnelly, J.P. (2005) Evidence of past intense tropical cyclones from backbarrier salt pond sediments: a case study from Isla De Culebrita, Puerto Rico, USA. *J. Coastal Res.*, **42**, 201–210.

Donnelly, J.P. & Woodruff, J.D. (2007) Intense hurricane activity over the past 5,000 years controlled by El Nino and the West African monsoon. *Nature*, **447**, 465–468.

Droxler, A.W. & Schlager, W. (1985) Glacial versus interglacial sedimentation rates and turbidite frequency in the Bahamas. *Geology*, **13**, 799–802.

Droxler, A.W., Morse, J.W. & Kornicker, W.A. (1988) carbonate mineral accumulation in Bahamian basins and adjacent Atlantic Ocean sediments. *J. Sediment, Petrol.*, **58**, 120–130.

Dunham, R.J. (1962) Classification of carbonate rocks according to depositional texture. In: *American Association of Petroleum Geologists Memoir 1* (Ed. by W.E. Ham), pp. 108–121. American Association of Petroleum Geologists, Tulsa, OK.

Fitzpatrick, S.M., Kaye, Q. & Kappers, M. (2004) A radiocarbon sequence for the Sabazan site, Carriacou, West Indies. *J. Caribbean Archaeol.*, **5**, 1–11.

Fratantoni, D.M., Zantopp, R.J., Johns, W.E. & Miller, J.L. (1997) Updated bathymetry of the Anegada-Jungfern Passage complex and implications for Atlantic inflow to the abyssal Caribbean Sea. *J. Mar. Res.*, **55**, 847–860.

García-Herrera, R., Gimeno, L., Ribera, P. & Hernández, E. (2005) New records of Atlantic hurricanes from Spanish documentary sources. *J. Geophys. Res.*, **110**, D03109. doi: 10.1029/2004JD005272.

Garrison, L., Holmes, C. & Trumbull, J. (1971) Geology of the insular shelf south of St. Thomas and St. John, Us Virgin islands. *US. Geological Survey Open-File Report*, 71–117, 38 p.

Gerhardt, S. & Henrich, R. (2001) Shell preservation of *Limacina inflata* (Pteropoda) in surface sediments from the central

and south Atlantic Ocean: a new proxy to determine the aragonite saturation state of water masses. *Deep Sea Res. Part I*, **48**, 2051–2071.

Van Gestel, J.P., Mann, P., Dolan, J.F. & Grindlay, N.R. (1998) Structure and tectonics of the upper Cenozoic Puerto Rico-Virgin Islands carbonate platform as determined from seismic reflection studies. *J. Geophys. Res.*, **103**, 30505–30530.

Gill, I., Mclaughlin, P.P. Jr & Hubbard, D.K. (1999) Evolution of the neogene kingshill basin of St. Croix, US Virgin Islands. In: *Sedimentary Basins of the World*, Vol. **4** (Ed. by P. Mann), pp. 343–366. Elsevier, Amsterdam.

Glaser, K.S. (1992) Late quaternary periplatform sediments and environments on the northeastern Nicaragua Rise, Caribbean Sea. PhD thesis, Rice University, Houston, 244 p.

Haddad, G.A. & Droxler, A.W. (1996) Metastable $CaCo_3$ dissolution at intermediate water depths of the Caribbean and western North Atlantic: implications for intermediate water circulation during the past 200,000 years. *Paleoceanography*, **11**, 701–716.

Handford, C.R. & Loucks, R.G. (1993) Carbonate depositional sequences and systems tracts-responses of carbonate platforms to relative sea-level changes. In: *Carbonate Sequence Stratigraphy Recent Developments and Applications* (Ed. by R.G. Loucks & J. Sarg) *Memoir*, **87**, 3–41. American Association of Petroleum Geologists, Tulsa, OK.

Hubbard, D.K. (1986) Sedimentation as a control of reef development: St. Croix, USVI. *Coral Reefs*, **5**, 117–125.

Hubbard, D.K. (1992) Hurricane-induced sediment transport in open-shelf tropical systems; an example from St. Croix, US Virgin Islands. *J. Sediment. Res.*, **62**, 946–960.

Hubbard, D.K., Suchanek, T., Gill, I., Cowper, S., Ogden, J.C., Westerfield, J.R. & Bayes, J. (1982) Preliminary studies of the fate of shallow-water detritus in the basin north of St. Croix. *Proceedings of the Fourth International Coral Reef Symposium*, Manila, Vol. 1, pp. 383–387.

Hubbard, D.K., Miller, A.I. & Scaturo, D. (1990) Production and cycling of calcium carbonate in a shelf-edge reef system (St. Croix, US Virgin Islands); applications to the nature of reef systems in the fossil record. *J. Sediment. Res.*, **60**, 335–360.

Hubbard, D.K., Zankl, H., Van Heerden, I. & Gill, I.P. (2005) Holocene reef development along the northeastern St. Croix Shelf, Buck Island, US Virgin Islands. *J. Sediment. Res.*, **75**, 97–113.

Hughen, K.A., Overpeck, J.T., Peterson, L.C. & Anderson, R.F. (1996) The nature of varved sedimentation in the Cariaco Basin, Venezuela, and its palaeoclimatic significance. In: *Palaeoclimatology and Palaeoceanography from Laminated Sediments* (Ed. by A.E.S. Kemp) *Geol. Soc. Spec. Publ.*, **116**, 171–183.

Inouchi, Y., Kinugasa, Y., Kumon, F., Nakano, S., Yasumatsu, S. & Shiki, T. (1996) Turbidites as records of intense palaeoearthquakes in Lake Biwa, Japan. *Sed. Geol.*, **104**, 117–125.

Joint Airborne LIDAR Bathymetry Technical Center of Expertise (JALBTCX) (2001) Vieques, Puerto Rico DVD. http://shoals.sam.usace.army.mil/.

Jany, I., Scanlon, K. & Mauffret, A. (1990) Geological interpretation of combined Seabeam, Gloria and seismic data from Anegada Passage (Virgin Islands, north Caribbean). *Mar. Geophys. Res.*, **12**, 173–196.

Johns, E., Wilson, W.D. & Molinari, R.L. (1999) Direct observations of velocity and transport in the passages between the Intra-Americas Sea and the Atlantic Ocean, 1984–1996. *J. Geophys. Res. Oceans (1978–2012)*, **104**, 25805–25820.

Johns, W.E., Townsend, T.L., Fratantoni, D.M. & Wilson, W.D. (2002) On the Atlantic inflow to the Caribbean Sea. *Deep Sea Res. Part I*, **49**, 211–243.

Jolly, W.T., Lidiak, E.G., Schellekens, J.H. & Santos, H. (1998) Volcanism, tectonics, and stratigraphic correlations in Puerto Rico. In: *Tectonics and Geochemistry of the Northeastern Caribbean* (Ed. by E.G. Lidiak & D.K. Larue) *Special Paper*, pp. 1–34. Geological Society of America, Boulder, CO.

Jorry, S.J., Droxler, A.W., Mallarino, G., Dickens, G.R., Bentley, S.J., Beaufort, L., Peterson, L.C. & Opdyke, B.N. (2008) Bundled turbidite deposition in the central Pandora Trough (Gulf of Papua) since Last Glacial Maximum: linking sediment nature and accumulation to sea level fluctuations at millennial timescale. *J. Geophys. Res. Earth Surface*, **113**, F01S19. doi: 10.1029/2006JF000649.

Jorry, S.J., Droxler, A.W. & Francis, J.M. (2010) Deepwater carbonate deposition in response to re-flooding of carbonate bank and atoll-tops at glacial terminations. *Quatern. Sci. Rev.*, **29**, 2010–2026.

Kastens, K.A. & Cita, M.B. (1981) Tsunami-induced sediment transport in the abyssal Mediterranean Sea. *Geol. Soc. Am. Bull.*, **92**, 845–857.

Kindinger, J.L., Miller, R.J. & Holmes, C.W. (1983) Sedimentology of Southwestern Roads region, US Virgin Islands; origin and rate of sediment accumulation. *J. Sediment. Res.*, **53**, 439–447.

Larue, D.K. (1994) Puerto Rico and the Virgin Islands. In: *Caribbean Geology, an Introduction* (Ed. by S.K.J. Donovan & T.A. Jackson), pp. 151–165. University of the West Indies Publishers' Association, Kingston.

Larue, D., Smith, A. & Schellekens, J. (1991) Oceanic island arc stratigraphy in the Caribbean region: don't take it for granite. *Sed. Geol.*, **74**, 289–308.

Larue, D., Torrini, R., Smith, A. & Joyce, J. (1998) North Coast Tertiary basin of Puerto Rico: from Arc basin to carbonate platform to arc-massif slope. In: *Tectonics and Geochemistry of the Northeastern Caribbean* (Ed. by E.G. Lidiak & D.K. Larue) *Special Paper*, pp. 155–176. Geological Society of America, Boulder, CO.

López-Venegas, A., Ten Brink, U.S. & Geist, E.L. (2008) Submarine landslide as the source for the October 11, 1918 Mona Passage tsunami: observations and modeling. *Mar. Geol.*, **254**, 35–46.

Lowe, D.R. (1982) Sediment gravity flows: II depositional models with special reference to the deposits of high-density turbidity currents. *J. Sediment. Res.*, **52**, 279.

Lowemark, L., Chen, H.F., Yang, T.N., Kylander, M., Yu, E.F., Hsu, Y.W., Lee, T.Q., Song, S.R. & Jarvis, S. (2010) Normalizing XRF-scanner data: a cautionary note on the interpretation of high-resolution records from organic-rich lakes. *J. Asian Earth Sci.*, **40**, 1250–1256.

Lyle, M. (1983) The brown-green color transition in marine sediments: a marker of the Fe (III)-Fe (II) redox boundary. *Limnol. Oceanogr.*, **285**, 1026–1033.

Masson, D., Harbitz, C., Wynn, R., Pedersen, G. & Løvholt, F. (2006) Submarine landslides: processes, triggers and hazard prediction. *Philos. Trans. A Math. Phys. Eng. Sci.*, **364**, 2009–2039.

McCann, W.R. (1985) On the earthquake hazards of Puerto Rico and the Virgin Islands. *Bull. Seismol. Soc. Am.*, **75**, 251–262.

McIlreath, I. & James, N. (1978) Facies models 13. Carbonate slopes. *Geosci. Can.*, **5**, 189–199.

Morton, R.W. (1973) Measurement of sediment sound velocity in carbonate sediments from the Whiting Basin, Puerto Rico, Naval Underwater Systems Laboratory. Newport, RI. TR4368.

Morton, R.W. (1975) Sound velocity in carbonate sediments from the Whiting Basin, Puerto Rico. *Mar. Geol.*, **19**, 1–17.

Mulder, T., Ducassou, E., Eberli, G., Hanquiez, V., Gonthier, E., Kindler, P., Principaud, M., Fournier, F., Léonide, P. & Billeaud, I. (2012) New insights into the morphology and sedimentary processes along the western slope of Great Bahama Bank. *Geology*, **40**, 603–606.

Mullins, H.T. & Hine, A.C. (1989) Scalloped bank margins: beginning of the end for carbonate platforms? *Geology*, **17**, 30–33.

Mullins, H.T. & Neumann, A.C. (1979) Deep carbonate bank-margin structure and sedimentation in the northern Bahamas. In: *Geology of Continental Slopes* (Ed. by L.J. Doyle & O.H. Pilkey) *SEPM Spec. Publ.*, **27**, 165–192.

Nakajima, T., Satoh, M. & Okamura, Y. (1998) Channel-levee complexes, terminal deep-sea fan and sediment wave fields associated with the Toyama Deep-Sea channel system in the Japan Sea. *Mar. Geol.*, **147**, 25–41.

NOAA Center for Coastal Monitoring & Assessment Biogeography Branch (2012). http://ccma.nos.noaa.gov/products/biogeography/usvi_nps/data/.

NOAA National Geophysical Data Center (2006) U.S. coastal relief model. Accessed April 2006, http://www.ngdc.noaa.gov/mgg/coastal/crm.html.

Oser, R. & Shumard, D. (1969) A sumarry of sediment size, composition, and engineering properties of 13 cores from Vieques Island, P.R.; December 1968 (USS Gillis); Laboratory Item 372, U.S. Naval Oceanographic Office. Washington, DC, 47.

Page, M.C. & Dickens, G.R. (2005) Sediment Fluxes to Marion Plateau (Southern Great Barrier Reef Province) over the last 130 Ky: new constraints on 'transgressive-shedding'off northeastern Australia. *Mar. Geol.*, **219**, 27–45.

Peltier, W. & Fairbanks, R.G. (2006) Global glacial ice volume and Last Glacial Maximum duration from an extended Barbados sea level record. *Quatern. Sci. Rev.*, **25**, 3322–3337.

Pilkey, O.H., Locker, S.D. & Cleary, W.J. (1980) Comparison of sand-layer geometry on flat floors of 10 modern depositional basins. *AAPG Bull.*, **64**, 841–856.

Poppe, L., Williams, S. & Paskevich, V. (2005) USGS East-Coast sediment analysis: procedures, database, and Gis data. US Geological Survey Open-File Report. 2005-1001.

Raussen, S., Lykke-Andersen, H. & Kuijpers, A. (2013) Tectonics of the Virgin Islands Basin, north eastern Caribbean. *Terra Nova*, **25**, 252–257.

Reid, H.F. & Taber, S. (1920) The Virgin Islands earthquakes of 1867–1868. *Bull. Seismol. Soc. Am.*, **10**, 9–30.

Reimer, P., Baillie, M., Bard, E., Bayliss, A., Beck, J., Blackwell, P., Ramsey, C.B., Buck, C., Burr, G. & Edwards, R. (2009) Intcal09 and Marine09 radiocarbon age calibration curves, 0–50,000 years cal Bp. *Radiocarbon*, **51**, 1111–1150.

Ridley, E., Stiles, N. & Nielson, G. (1963) Oceanography-West Coast of St. Croix, Virgin Islands, U.S. Naval Oceanographic Office. Washington, DC, 88 p.

Robson, G. (1964) An earthquake catalogue for the eastern Caribbean 1530–1960. *Bull. Seismol. Soc. Am.*, **54**, 785–832.

Rooney, R.F., Eppert, H.C. & Huddell, H.D. (1965) A summary of engineering properties, size, and composition of cores from St. Croix and Puerto Rico, October 1965; Laboratory Item 280, U.S. Naval Oceanographic Office. Washington, DC.

Ross, C., Kelly, E., Reynolds, L. & Bowman, J. (1976) A summary of sediment size, sound velocity and mass physical and engineering properties of 22 cores from the Caribbean, USS Kane, February 1976; Laboratory Item 496, U.S. Naval Oceanographic Office. Washington, DC, 61.

Rothwell, R.G., Hoogakker, B., Thomson, J., Croudace, I.W. & Frenz, M. (2006) Turbidite emplacement on the southern Balearic Abyssal Plain (Western Mediterranean Sea) during marine isotope stages 1–3: an application of Itrax XRF scanning of sediment cores to lithostratigraphic analysis. In: *New Techniques in Sediment Core Analysis* (Ed. by R.G. Rothwell) *Geol. Soc. Spec. Publ.*, **267**, 79–89.

Rusnak, G.A. & Nesteroff, W. (1964) Modern turbidites: terrigenous abyssal plain versus bioclastic basin. In: *Papers in Marine Geology, Shepard Commemerative Volume* (Ed. by R. Miller), pp. 488–507. Macmillan, New York.

Sar, E. & Ça Atay, M.N. (2006) Turbidites and their association with past earthquakes in the deep Ç Narc K Basin of the Marmara Sea. *Geo-Mar. Lett.*, **26**, 69–76.

Schellekens, J.H. (1998) Geochemical evolution and tectonic history of Puerto Rico. In: *Tectonics and Geochemistry of the Northeastern Caribbean* (Ed. by E.G. Lidiak & D.K. Larue) *Geol. Soc. Am. Spec. Pap.*, **322**, 35–66.

Schlager, W. & Chermak, A. (1979) Sediment facies of platform-basin transition, Tongue of the Ocean, Bahamas. In: *Geology of Continental Slopes* (Ed. by L.S. Doyle & O.H. Pilkey Jr.) *Soc. Econ. Paleontol. Mineral. Spec. Publ.*, **27**, 193–208.

Schlager, W., Reijmer, J.J.G. & Droxler, A. (1994) Highstand shedding of carbonate platforms. *J. Sediment. Res.*, **64**, 270–281.

Schneidermann, N., Pilkey, O.H. & Saunders, C. (1976) Sedimentation on the Puerto Rico insular shelf. *J. Sediment. Res.*, **46**, 167–173.

Seiglie, G.A., Froelich, P.N. & Pilkey, O.H. (1976) Deep-sea sediments of Navidad Basin: correlation of sand layers. *Deep Sea Res.*, **23**, 89–101.

Sexton, P.F. & Norris, R.D. (2011) High latitude regulation of low latitude thermocline ventilation and planktic foraminifer populations across glacial-interglacial cycles. *Earth Planet. Sci. Lett.*, **311**, 69–81.

Shanmugam, G. (1997) The Bouma sequence and the turbidite mind set. *Earth Sci. Rev.*, **42**, 201–229.

Shanmugam, G. & Moiola, R. (1984) Eustatic control of calciclastic turbidites. *Mar. Geol.*, **56**, 273–278.

Shepard, F.P. (1979) Submarine slopes and canyons on North Side St. Croix Island. *Mar. Geol.*, **31**, M69–M76.

Smith, T., Blondeau, J., Nemeth, R., Pittman, S., Calnan, J., Kadison, E. & Gass, J. (2010) Benthic structure and cryptic mortality in a caribbean mesophotic coral reef bank system, the Hind Bank Marine Conservation District, Us Virgin Islands. *Coral Reefs*, **29**, 289–308.

Speed, R. (1989) Tectonic evolution of St. Croix: implications for tectonics of the northeastern Caribbean. In: *Terrestrial and Marine Geology of St. Croix, Us Virgin Islands* (Ed. by D.K. Hubbard) *Special Publication N.8*, pp. 9–22. West Indies Laboratory, Teague Bay, St. Croix.

Speed, R. & Joyce, J. (1989) Depositional and structural evolution of cretaceous strata, St. Croix. In: *Terrestrial and Marine*

Geology of St. Croix, US Virgin Islands, West Indies Laboratory (Ed. by D.K. Hubbard) *Special Publication*, **8**, 23–36.

Stanley, D.J. (1981) Unifites: structureless muds of gravity-flow origin in mediterranean basins. *Geo-Mar. Lett.*, **1**, 77–83.

St-Onge, G., Mulder, T., Piper, D.J.W., Hillaire-Marcel, C. & Stoner, J.S. (2004) Earthquake and flood-induced turbidites in the Saguenay Fjord (QuÉbec): a Holocene paleoseismicity record. *Quatern. Sci. Rev.*, **23**, 283–294.

Stow, D.A.V., Howell, D.G. & Nelson, C.H. (1983) Sedimentary, tectonic, and sea-level controls on submarine fan and slope-apron turbidite systems. *Geo-Mar. Lett.*, **3**, 57–64.

Strasser, M., Stegmann, S., Bussmann, F., Anselmetti, F.S., Rick, B. & Kopf, A. (2007) Quantifying subaqueous slope stability during seismic shaking: Lake Lucerne as model for ocean margins. *Mar. Geol.*, **240**, 77–97.

Stuiver, M. & Reimer, P.J. (1993) Extended ^{14}C database and revised Calib Radiocarbon calibration program. *Radiocarbon*, **35**, 215–230.

ten Brink, U.S. & Lopez-Venegas, A.M. (2012) Plate interaction in the NE Caribbean subduction zone from continuous GPS observations. *Geophys. Res. Lett.*, **39**, L10304.

ten Brink, U.S., Bakun, W.H. & Flores, C.H. (2011) Historical perspective on seismic hazard to Hispaniola and the northeast Caribbean region. *J. Geophys. Res.*, **116**, B12318.

ten Brink, U., Coleman, D.F., Chaytor, J., Demopoulos, A.W.J., Armstrong, R., Garcia-Moliner, G., Raineault, N.A., Andrews, B., Chastain, R., Rodrigue, K. & Mercier-Gingras, M. (2014) Earthquake, landslide, and tsunami hazards and benthic biology in the Greater Antilles. *Oceanography*, **27** (supplement), 34–35.

Tripsanas, E.K., Bryant, W.R. & Phaneuf, B.A. (2004) Depositional processes of uniform mud deposits (unifites), Hedberg Basin, northwest Gulf of Mexico: new perspectives. *AAPG Bull.*, **88**, 825–840.

Webster, J.M., Beaman, R.J., Puga-Bernabéu, Á., Ludman, D., Renema, W., Wust, R.A., George, N.P., Reimer, P.J., Jacobsen, G.E. & Moss, P. (2012) Late Pleistocene history of turbidite sedimentation in a submarine canyon off the northern Great Barrier Reef, Australia. *Palaeogeogr. Palaeoclimatol. Palaeoecol.*, **331**, 75–89.

Whetten, J.T. (1966) Geology of St. Croix, U.S. Virgin Islands. In: *Caribbean Geological Investigations*, Vol. **98** (Ed. by H.H. Hess), pp. 177–239. Geological Society of America, Boulder, CO.

Wynn, R.B., Masson, D.G., Stow, D.A.V. & Weaver, P.P.E. (2000) Turbidity current sediment waves on the submarine slopes of the western Canary Islands. *Mar. Geol.*, **163**, 185–198.

Manuscript received 17 July 2013; In revised form 22 April 2014; Manuscript accepted 18 May 2014.